EXPERIMENTAL INVESTIGATION OF ENERGY DISSIPATION THROUGH INCLINED SCREENS

A THESIS SUBMITTED TO
THE GRADUATE SCHOOL OF NATURAL AND APPLIED SCIENCES
OF
MIDDLE EAST TECHNICAL UNIVERSITY

BY

GÖRKEM BALKIŞ

IN PARTIAL FULFILLMENT OF THE REQUIREMENTS
FOR
THE DEGREE OF MASTER OF SCIENCE
IN
CIVIL ENGINEERING*

SEPTEMBER 2004

Approval of the Graduate School of Natural and Applied Sciences

_____

Prof. Dr. Canan ÖZGEN
Director

I certify that this thesis satisfies all the requirements as a thesis for the degree of Master of Science.

_____

Prof. Dr. Erdal ÇOKÇA
Head of Department

This is to certify that we have read this thesis and that in our opinion it is fully adequate, in scope and quality, as a thesis for the degree of Master of Science.

Prof. Dr. Metin Ger	Assist. Prof. Dr. Zafer Bozkuş
Co-Supervisor	Supervisor

Examining Committee Members

Prof. Dr. Cahit ÇIRAY	(METU, AE)	_____
Assist. Prof. Dr. Zafer Bozkuş	(METU, CE)	_____
Prof. Dr. Doğan ALTINBİLEK	(METU, CE)	_____
Prof. Dr. Metin GER	(METU, CE)	_____
Dr. Şahnaz TİĞREK	(METU, CE)	_____

I hereby declare that all information in this document has been obtained and presented in accordance with academic rules and ethical conduct. I also declare that, as required by these rules and conduct, I have fully cited and referenced all material and results that are not original to this work.

Name, Last name :Görkem BALKIŞ

Signature :

ABSTRACT

EXPERIMENTAL INVESTIGATION OF ENERGY DISSIPATION THROUGH INCLINED SCREENS

Balkış, Görkem
M.Sc., Department of Civil Engineering
Supervisor: Assist. Prof. Dr. Zafer Bozkuş
Co-Supervisor: Prof. Dr. Metin Ger

September 2004, 76 pages

The main goal of the present study is to investigate the energy dissipation through inclined screens. Recent studies have shown that screens arranged vertically may dissipate more energy than a hydraulic jump does below small hydraulic structures. In the present study a series of laboratory experiments were performed in order to determine the effect of inclination of the screen on the energy dissipated by the screen. The porosity of the screen used in the experiments is 40%. Inclination angle, thickness of the screen, location of the screen, upstream flow depth, and the Froude number of the upstream flow are the major parameters for the laboratory experiments. Froude number of the upstream flow covered a range of 5 to 24. A screen was located up to a distance 100 times the undisturbed upstream flow depth from the gate and the thickness of the screen was changed in correlation with the depth of upstream flow. The results of the experiments show that the inclination parameter has an insignificant effect on the energy dissipated by the screen. Namely, inclination of the screen does not contribute much in reducing the energy of the flowing water further, compared to vertically placed screens.

Keywords: Screen, energy dissipation, inclination, porosity, hydraulic jump

ÖZ

EĞİK ELEKLERLE ENERJİ KIRILIMININ DENEYSEL OLARAK ARAŞTIRILMASI

Balkış, Görkem
Yüksek Lisans, İnşaat Mühendisliği Bölümü
Tez Danışmanı: Yar. Doç. Dr. Zafer Bozkuş
Yardımcı Tez Danışmanı: Prof. Dr. Metin Ger

Eylül 2004, 76 sayfa

Bu çalışmanın ana amacı eğik eleklerde enerji kırılımının araştırılmasıdır. Yakın geçmişte yapılan araştırmalar küçük hidrolik yapıların mansabında dikey olarak yerleştirilmiş eleklerin hidrolik sıçramaya oranla daha çok enerji kırdığını göstermiştir. Bu tezde eleğin eğikliliğinin enerji kırılımına etkisini ortaya çıkarmak amacıyla bir dizi deney yapılmıştır. Deneylerde kullanılan eleklerin boşluk oranı %40'dır. Eğiklik açısı, elek kalınlığı, eleğin yeri, menba su derinliği ve menba akımının Froude sayısı laboratuar deneyleri için esas parametrelerdir. Menba akımının Froude sayıları 5 ile 24 arasında değişmektedir. Elek, menba su derinliğinin 100 katına kadar olan uzaklıklarda yerleştirilmiştir ve elek kalınlığı menba su derinliği ile ilişkili olarak değiştirilmiştir. Deney sonuçları, eğiklik parametresinin elek tarafından kırılan enerji üzerindeki etkisinin önemsiz olduğunu göstermektedir. Yani eleğin elekliğinin, dik koyulan eleklere kıyasla, akan suyun enerjisinin biraz daha azaltılmasına pek katkısı yoktur.

Keywords: Elek, enerji kırılımı, eğiklik, boşluk oranı, hidrolik sıçrama

To my mother, Süheyla Balkış…

ACKNOWLEDGMENTS

I wish to express my deepest gratitude to my supervisor; Assist. Prof. Dr. Zafer Bozkuş for his guidance, support and encouragement throughout my research.

I would like to thank Prof. Dr. Metin Ger for his constructive discussions during my study.

I am deeply grateful to Research Assistant Yavuz Özeren for his generous support during the experimental phase of the study.

I would like to thank Mr.Yunus Emre Ulukütük for his understanding and support during my study.

Finally, I would like to express my deepest gratitude to my family for their love and invaluable support throughout my whole life.

TABLE OF CONTENTS

LIST OF TABLES

LIST OF FIGURES

LIST OF SYMBOLS

A_0	area of Section 0 of the orifice-meter
A_1	area of Section 1 of the orifice-meter
A_2	area of Section 2 of the orifice-meter
C_0	discharge coefficient of the orifice-meter
C_C	contraction coefficient of the orifice-meter
C_V	contraction coefficient of vena contracta
d	gate opening
D_0	orifice throat diameter
D_1	pipe diameter in which the orifice meter is mounted
D_{hole}	diameters of the screen holes
E_G	energy at section G
Fr_A	Froude number at Section A
Fr_C	Froude number at Section C
Fr_G	Froude number at Section G
g	gravitational acceleration
h_L	head loss through the orifice-meter
k	distance between the screens of the double screen
L	theoretical length of a full jump
p	porosity of the screen
p_1	pressure at Section 1 of the orifice-meter
p_2	pressure at Section 2 of the orifice-meter
Q	flow rate
Q_{ideal}	ideal discharge for the orifice-meter
Re	Reynold's number
S	energy dissipated due to screen
t	thickness of the screen
V_1	velocity at Section 1 of the orifice-meter
V_2	velocity at Section 2 of the orifice-meter

V_A	average velocity at Section A
V_C	average velocity at Section C
w	width of the channel
X	distance between the screen and the gate
x	distance from the upstream end of the pseudo-jump to the screen
y_A	water depth at Section A
y_{A2}	conjugate depth of y_A
y_C	water depth at Section C
y_G	water depth at Section G
ΔE_{AB}	energy loss between Sections A and B
ΔE_{AC}	energy loss between Sections A and C
ΔE_{GC}	energy loss between Sections G and C
ΔE_{jA}	energy loss due to a full jump at Section A
ΔE_{jG}	energy loss due to a full jump at Section G
α	a non-dimensional parameter defined in Equation 3.3
β	a non-dimensional parameter defined in Equation 3.2
ϕ	diameter ratio of the Sections 0 and 1 for the orifice-meter
γ	specific weight of water
η_{scr}	screen efficiency
η_{sys}	system efficiency
μ	dynamic viscosity of water
ρ	density of water
θ	inclination angle of screen

CHAPTER I

INTRODUCTION

The energy of water is one of the most fundamental subjects that hydraulic engineering deals with. Most of the efforts of the engineers have been on the controlling of that energy. These efforts have resulted in developing control structures, which are sometimes used to dissipate energy and its destructive effects, and sometimes to utilize this energy for the benefit of the society. Most of the control structures, designed to dissipate the energy of the water uses the hydraulic jump action and its energy dissipative effects. Stilling basins are the most common structures of this type of structure. Whichever the type of structure is, the effectiveness of the control structures is mostly related with the amount of energy that they can dissipate. As a result, engineers are trying to improve the effectiveness of the structures, namely, their ability to dissipate the energy of flowing water, and this results in studies for finding new methods and structures to be used for energy dissipation.

In recent years, an alternative method for dissipating energy rather than hydraulic jump has been investigated; the screens. According to the studies of the hydraulic engineers, screens may dissipate more energy than a hydraulic jump can. The present study is conducted in order to find out how the efficiency, which is the energy dissipative capability of screens, can be increased. An additional parameter, inclination angle of the screens, which was not considered in the previous studies, was taken into consideration in order to determine the effects of that parameter on the energy dissipative effects of the screens.

Firstly, dimensional analysis was performed in order to specify major non dimensional parameters that would be taken into account during the laboratory experiments. As a result of dimensional analysis major non dimensional parameters have been determined as Froude number of the upstream flow, relative location of the screen, relative thickness of the screen and inclination of the screen. After that, laboratory experiments were conducted according to the non dimensional parameters determined during the dimensional analysis stage.

Experiments are carried out for a wide range of Froude numbers from 5 to 24. The screen with a porosity of 40% was used for the experiments. And the location of the screen was arranged as 50 and 100 times of the undisturbed upstream flow depth from the gate.

Chapter II is a brief summary of the literature review of the previous studies related to the screens in hydraulic engineering. Chapter III is the conceptual description of the subject. In Chapter IV, details of the laboratory experiments were described. Chapter V focuses on the results and discussions of the laboratory experiments. Finally, the conclusions were presented in Chapter VI.

CHAPTER II

LITERATURE REVIEW

The most recent studies that are directly related with the concept of using screens as energy dissipaters as an alternative to hydraulic jump are those by Rajaratnam and Hurtig (2000) and Çakır (2003). Consequently, the present study is a follow up study in order to enhance the understanding of the subject of "energy dissipation created by the screens" by including inclination as a new parameter to these parameters which were used in the more recent studies. Here below, the two most recent studies related to this subject are summarized.

As triangular and double screens have been used against erosion for roadside ditches and other steep land surfaces, Rajaratnam and Hurtig (2000*)* had made investigation on energy dissipation through these screens. Three types of screens were used in their laboratory experiments; single screen, double screen and triangular screen. Double screen is formed by placing two screens with a 75 mm gap between them. Triangular screen was formed by connecting two screens with an apex angle of 60˚. Both types of screens were placed perpendicularly across the supercritical flow and it was observed that both types of the screens dissipated significant amount of energy. Screens used had an areal porosity of 40%. This porosity was generated using roughly square holes (of 5 mm sides). The Froude number of the upstream flow varied from 5 to 13.

A rectangular channel on which the first series of experiments were conducted was 0.45 m wide, 0.43 m deep, and 6.3 m long. For the first series of experiments, water was supplied from a water tank with a sharp–edged sluice gate.

Another rectangular channel on which the second series of experiments were performed was 0.305 m wide, 0.7 m deep and 6 m long with a sluice gate fitted with a streamlined bottom.

As a result of these experiments it was concluded that screens or porous baffles with a porosity of about 40% could be used as effective energy dissipaters below hydraulic structures, either as a single screen, double screen or triangular screen. Results showed that energy dissipation by screens was larger than that produced by the hydraulic jump. By these experiments, it was observed that three kinds of water action took place at the upstream flow; free hydraulic jumps, forced hydraulic jumps, and submerged jumps. The flow leaving these screens was found to be supercritical with a Froude number approximately equal to 1.65 and a tail water depth equal to 0.28 times the subcritical sequent depth of the hydraulic jump with the same Froude number.

Another investigation on the subject was recently done by Çakır (2003) conducting laboratory experiments in order to determine the energy dissipation through screens. Major parameters used for these experiments are the Froude number of the upstream flow, porosity of the screens, thickness of the screens and location of the screens. The screens used for the experiments had the porosities of 40%, 50%, and 60%. Location of the screens was changed up to 100 times the upstream flow depth away from the gate. For laboratory experiments 2 cm thick screen, 4 cm thick screen, and two double screen configuration formed by two screens having 1 cm and 2 cm gap between them were used. The Froude number of upstream flow varied between 5 and 18. In the experiments, a pressurized tank with a gate at its bottom was used to supply water to the channel. The gate opening was adjusted in order to change the upstream flow depth. Flow depth was measured by a point gage at various locations along the channel.

Findings of Çakır (2003) were presented by Bozkuş et al. (2004) in which it was concluded that;

- The system performance which is defined by the relative energy loss; $\Delta E_{GC} / E_{G,}$ increases with increasing Froude number,

  where E_G is the total energy at point G and ΔE_{GC} is the total energy loss between just downstream of the gate (i.e. point G) and just downstream of the screen (i.e. point C)

- Efficiency of system decreases with increasing Froude number

- Screens with 40% porosity gives higher energy dissipation

- Double screens dissipate more energy than single screens

- When screens were compared with stilling basins with their energy dissipative capacity, screens were found to be more efficient than stilling basins.

CHAPTER III

CONCEPTUAL FRAME

As it was stated before, the main aim of the present study is to determine the energy dissipation through the screens located downstream of a small hydraulic structure and the effect of screen inclination parameter on the system efficiency. A pressurized tank with a gate was used in order to simulate the small hydraulic structure.

3.1 Theoretical Aspect

According to the observations done during the laboratory experiments, the flow at the upstream of the screen can be classified as follows:

Case 1: The effect of the screen on the upstream flow results in a fully formed hydraulic jump. That means; the distance between the point where jump begins and the screen is long enough to lead to a complete hydraulic jump, Figure 3.1. Since the length of a jump is directly related with the Froude number of the flow at the point where the hydraulic jump begins, this flow behavior is observed at low Froude numbers.

The length of a jump is given by French (1986), as

$$L=9.75y_A(Fr_A-1)^{1.01} \tag{3.1}$$

where

$$Fr_A=\frac{V_A}{\sqrt{gy_A}} \tag{3.2}$$

in which y_A, Fr_A, V_A are the flow depth, Froude number and flow velocity respectively at section A and g is the gravitational acceleration.

And for this case;

$$L \leq x \tag{3.3}$$

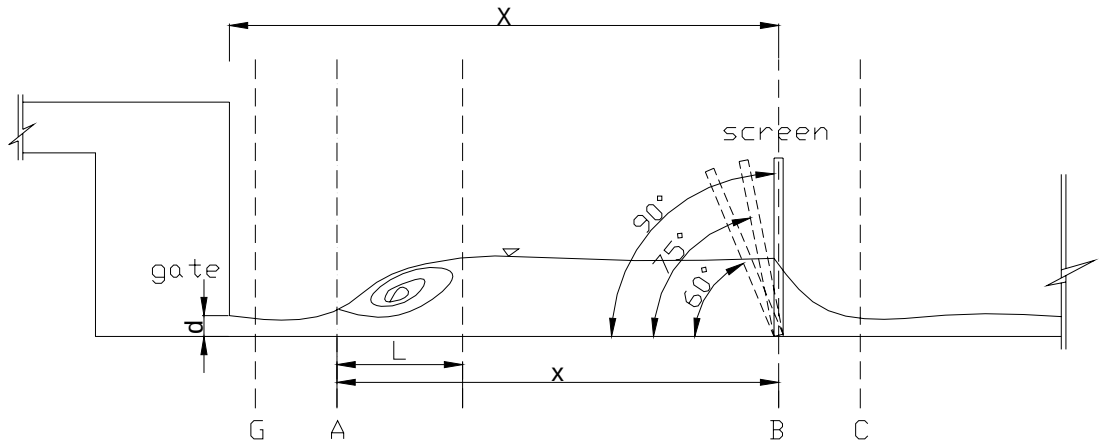

Figure 3.1 General Sketch of the flow for Case 1

Figure 3.2 Sample view for upstream flow of Case 1

Figure 3.3 Sample view for downstream flow of Case 1

Figure 3.4 Sample view for Case 1

Case 2: The effect of the screen on the upstream flow results in a pseudo hydraulic jump. That means, the distance between the point where the jump begins and the screen is not long enough to lead to a complete hydraulic jump, Figure 3.5. This flow behavior is observed at high Froude numbers.

After comparing both of the cases, it was observed that the energy dissipation for the second case is much higher than the first case. Consequently, in the present study main focus was placed on the second case. However, the first case was also included for the sake of completeness.

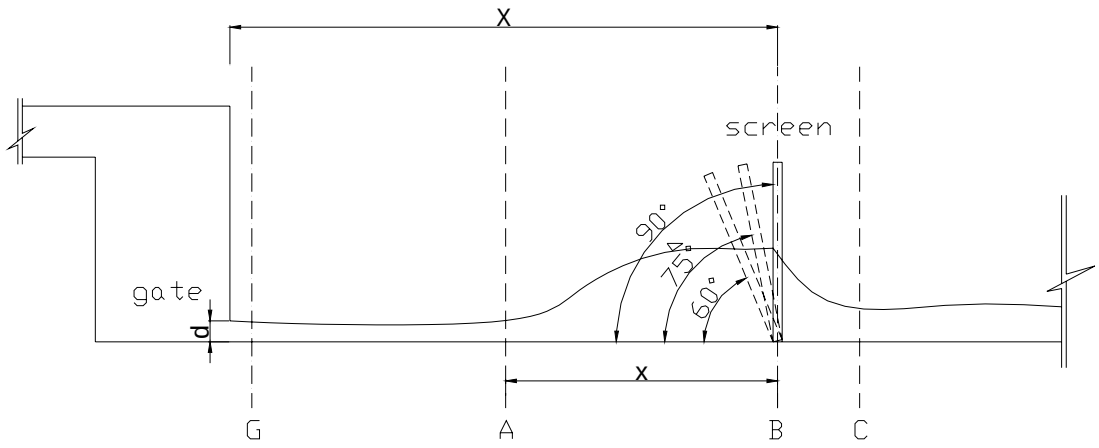

Figure 3.5 General Sketch of the flow for Case 2

Figure 3.6 Sample view of inclined screens for Case 2

Figure 3.7 Sample view of vertical screens for Case 2

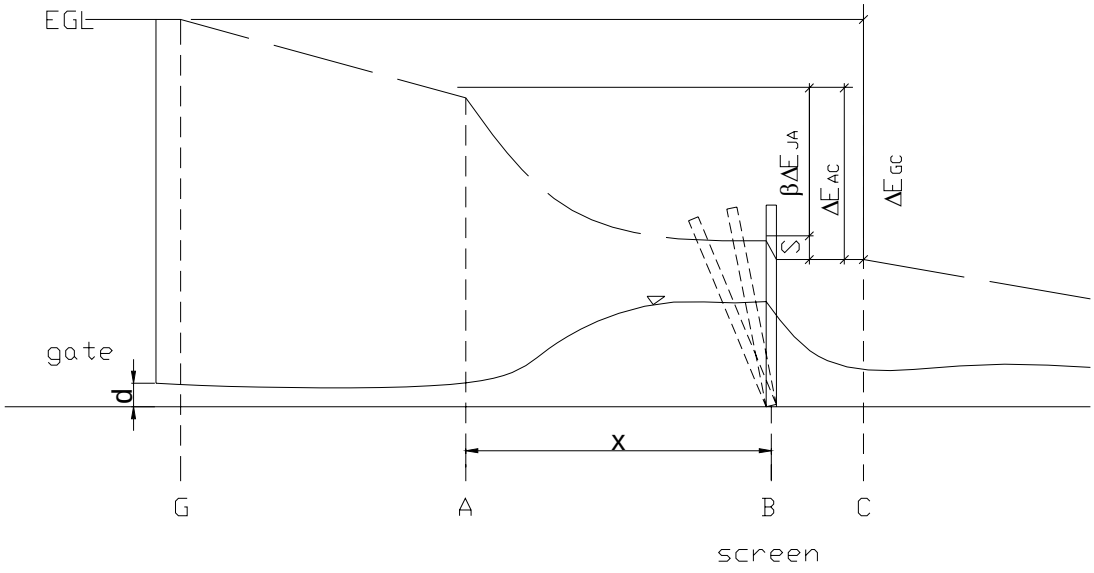

Figure 3.8 Energy loss definitions

The energy loss computations are performed by using the following approach after Çakır (2003).

$$\Delta E_{JA} = (y_A + \frac{V_A^2}{2g}) - (y_{A2} + \frac{V_{A2}^2}{2g}) \quad (3.4)$$

where ΔE_{JA} is defined as the energy loss due to a full jump that could be formed at section A, y_A is the flow depth at section A, y_{A2} is the subcritical sequent depth of flow and V_{A2} is the velocity of the flow at the section where y_{A2} occurs.

For the complete hydraulic jump case, energy loss due to a hydraulic jump is equal to the energy loss between points A and B

$$\Delta E_{AB} = \Delta E_{JA} \quad (3.5)$$

And for the pseudo-hydraulic jump case energy loss due to a pseudo-jump can be computed by using the below expressions.

$$\Delta E_{AB} = \beta \Delta E_{JA} \quad (3.6)$$

where β was developed by Çakır (2003) as

$$\beta = e^{(1-\frac{1}{\alpha})} \quad (3.7)$$

$$\alpha = \frac{x}{L} \quad (3.8)$$

$$0 < \beta < 1 \quad (3.9)$$

The system loss is computed as follows;

$$\Delta E_{GC} = (y_G + \frac{V_G^2}{2g}) - (y_C + \frac{V_C^2}{2g}) \quad (3.10)$$

$$y_G = C_V \cdot d \tag{3.11}$$

where C_V=0.625 after Simon (1981)

The energy loss at the screen is computed as follows;

$$S = \Delta E_{AC} - \Delta E_{AB} \tag{3.12}$$

or it can be rewritten as

$$S = (y_A + \frac{V_A^2}{2g}) - (y_C + \frac{V_C^2}{2g}) - \beta \Delta E_{jA} \tag{3.13}$$

where y_C and V_C are the flow depth and velocity respectively at Section C.

Efficiency of the system is evaluated as follows:

$$\eta_{sys} = \frac{\Delta E_{GC} - \Delta E_{jG}}{\Delta E_{jG}} \tag{3.14}$$

where ΔE_{JG} is defined as energy loss due to a full jump that could be formed at section G.

And the efficiency of the screen is defined as

$$\eta_{scr} = \frac{S}{\Delta E_{jG}} \tag{3.15}$$

3.2 Dimensional Analysis

In order to conduct the experiments in the most efficient manner the most relevant physical quantities of the energy dissipation problem were identified.

They are listed below along with their dimensions.

S: energy head dissipated due to screen, [L],

Q: discharge, [L^3T^{-1}],

d: gate opening, [L],

w: width of the channel, [L],

y_G: water depth at Section G, [L],

y_A: water depth at Section A, [L],

y_C: water depth at Section C, [L],

x: the distance from the upstream end of the pseudo-jump to the screen, [L],

X: distance between the screen and the gate, [L],

p: porosity of the screen,

k: distance between the screens of the double screens, [L],

t: thickness of the screen, [L],

g: gravitational acceleration, [LT^{-2}],

ρ:density of water, [ML^{-3}],

μ: dynamic viscosity of water, [$ML^{-1}T^{-1}$)]

θ: Inclination angle,

Basic equation of the system is expressed as below;

$$S = f_1(Q, d, w, y_G, y_A, y_C, x, X, p, k, t, g, \rho, \mu, \theta) \tag{3.16}$$

As Çakır (2003) described;

If one recalls the fact that E_G, energy at section G, and the slug length L (both having the length dimension) and Fr_C, Froude number just downstream the screen, are functions of

$$L = f_2(g, w, Q, y_A) \tag{3.17}$$

$$Fr_C = f_3(g, w, Q, y_C) \tag{3.18}$$

$$E_G = f_4(g, y_G, d, w, Q) \tag{3.19}$$

We can rewrite Equation 3.16 by incorporating Equations 3.17, 3.18 and 3.19 in place of w, y_A and y_C as

$$S = f_5(Q, d, E_G, y_G, L, Fr_C, x, X, p, k, t, g, \rho, \mu, \theta) \tag{3.20}$$

After the dimensional analysis was performed by using y_G, g and ρ as repeating variables the following dimensionless relationship was obtained:

$$\frac{S}{y_G} = f_6\left(\frac{E_G}{y_G}, Fr_G, \frac{L}{y_G}, Fr_C, \frac{x}{y_G}, \frac{X}{y_G}, p, \frac{k}{y_G}, \frac{t}{y_G}, \frac{d}{y_G}, Re, \theta\right) \tag{3.21}$$

where Re is the Reynolds number.

The equation above was re-oriented and the equation below was obtained.

$$\frac{S}{E_G} = f_7\left(Fr_G, \alpha, \frac{X}{d}, \frac{k}{d}, \frac{t}{d}, \theta, \middle| p, Fr_C, \frac{E_G}{d}, \frac{x}{d}, C_V, Re\right) \tag{3.22}$$

As Çakır (2003) stated;

"The three of the last five parameters namely Fr_C, $\frac{E_G}{d}$, and $\frac{x}{d}$ are irrelevant to the scope of this study. C_V, which is defined as $\frac{y_G}{d}$ is a constant. As to the *Re*, the magnitude of Fr_G is relatively high in the range covered during the experiments therefore there is no dependence of the flow behavior on the Reynolds number."

Furthermore, based on the findings of Rajaratnam and Hurtig and Çakır, it was assumed that optimum porosity of 40% would be valid for the range of inclinations studied, *p* was also dropped out of the equation as variable.

Consequently, experimental procedure was established based on the following dimensionless parameters; $Fr_G, \alpha, \frac{X}{d}, \frac{k}{d}, \frac{t}{d}, \theta$.

CHAPTER IV

LABORATORY WORK

In this chapter experimental setup and the procedure selected according to the dimensional analysis were explained.

4.1 Experimental Setup

A horizontal rectangular channel of 7.5 m long was used for the experiments, Figure 4.1. The channel had a width of 29 cm and a height of 70 cm. Water is supplied from a constant head tank and transmitted to the pressurized tank by a pipe whose diameter is 206 mm. The discharge measurements are obtained by using the orifice meter installed on this pipe. Also there is a valve on the pipe just before its entrance to the pressurized tank by which discharge can be adjusted during the measurements. The pressurized tank has a gate at its bottom, which is used to vary upstream flow depth. The flow depth measurements are taken by a mobile point gage. A porosity of the screens used in the experiments was fixed at a value of 40%. The device, which is assembled at the top of the screen, enables various inclinations of the screen. A schematic view of the experimental setup is provided in Figures 4.1, 4.2 and 4.3.

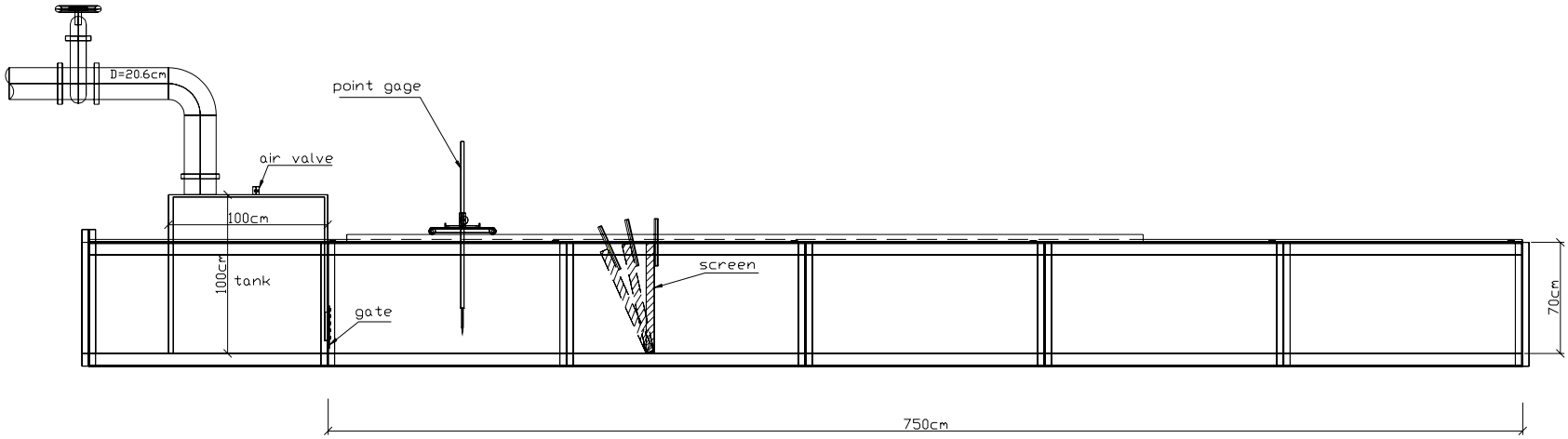

Figure 4.1 Side view of experiment setup

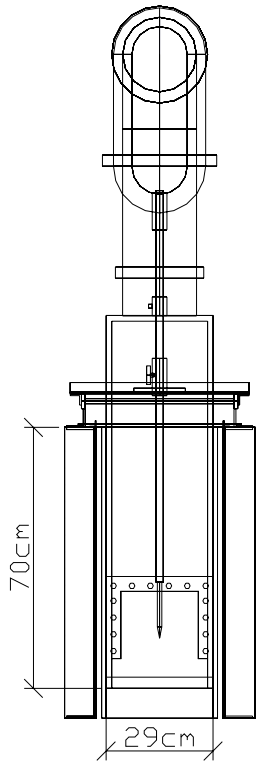

Figure 4.2 Front view of experiment setup (After Çakır, 2003)

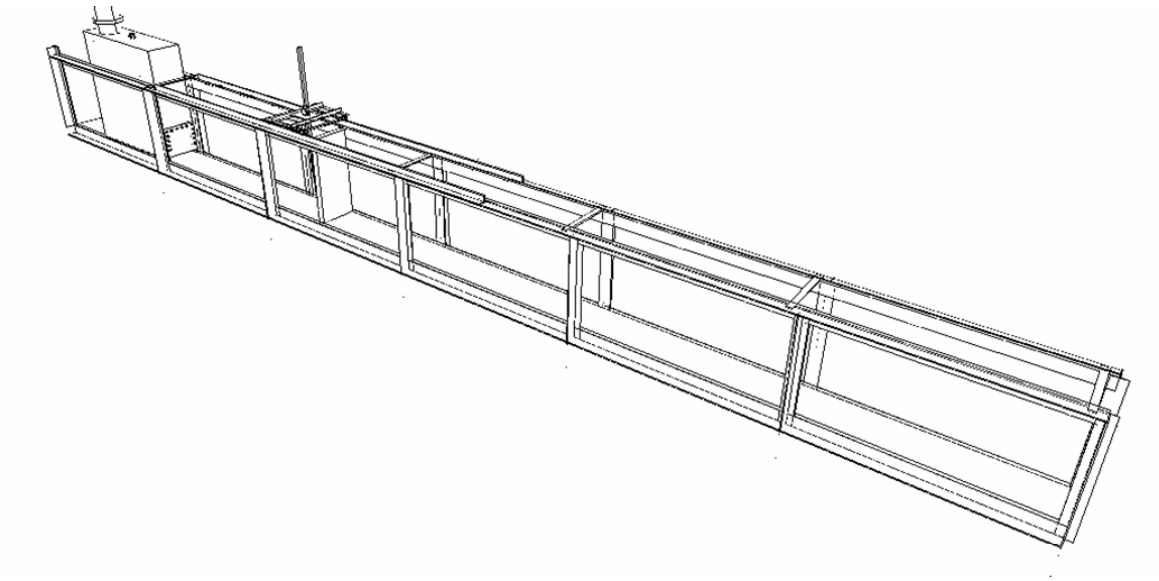

Figure 4.3 A general view of experiment setup (After Çakır, 2003)

4.1.1 Gate

Water is released from the pressurized tank into the channel by a gate with a rectangular cross section. The height of the gate opening is adjusted during the experiments in order to obtain the required heights in correlation with the t/d parameter specified in the dimensional analysis. Two different heights of gate opening are used for the experiments, namely 2 cm and 4 cm.

4.1.2 Screens

Screens are made of Plexiglas and each one has a thickness of 1 cm and a porosity of 40%. The porosity was obtained by the 1 cm diameter holes arranged with a uniform triangular mesh. For the laboratory experiments, two screens were placed back to back in order to form a screen with a thickness of 2 cm with no gap between them. Similarly, four screens were put together to form a screen with a thickness of 4 cm with no gap between them, and two screens were connected with a 2 cm gap between them in order to form a double screen. The screen was mounted in the channel by fixing both its bottom and top. It was fixed to the channel bottom by a screw and to the top of the channel by a mechanism, which allows it to be inclined. During the experiments, the inclination angle was changed by the help of this mechanism. The other parameters that are changed in order to determine their effects are the relative location of the screen according to the *X/d* ratio and as explained before, the relative thickness of the screens, *t/d*. Figure 4.4 shows the configuration of a typical screen.

4.1.3 Orifice meter

The discharge measurements were obtained by using an orifice meter designed and assembled according to the Institution of Turkish Standards (TSE) specifications. It is located on the pipe, which transmits the water from the constant head tank to the pressurized tank. The orifice meter includes a mercury manometer inclined with an angle of 30˚. Determination of discharge by the orifice used in the experiments is explained in detail in Appendix A. During the measurements,

discharge can be varied by using a valve located on the same pipe. All other detailed information including the orifice curve, correction coefficient charts and schematic representation are covered in Appendix A.

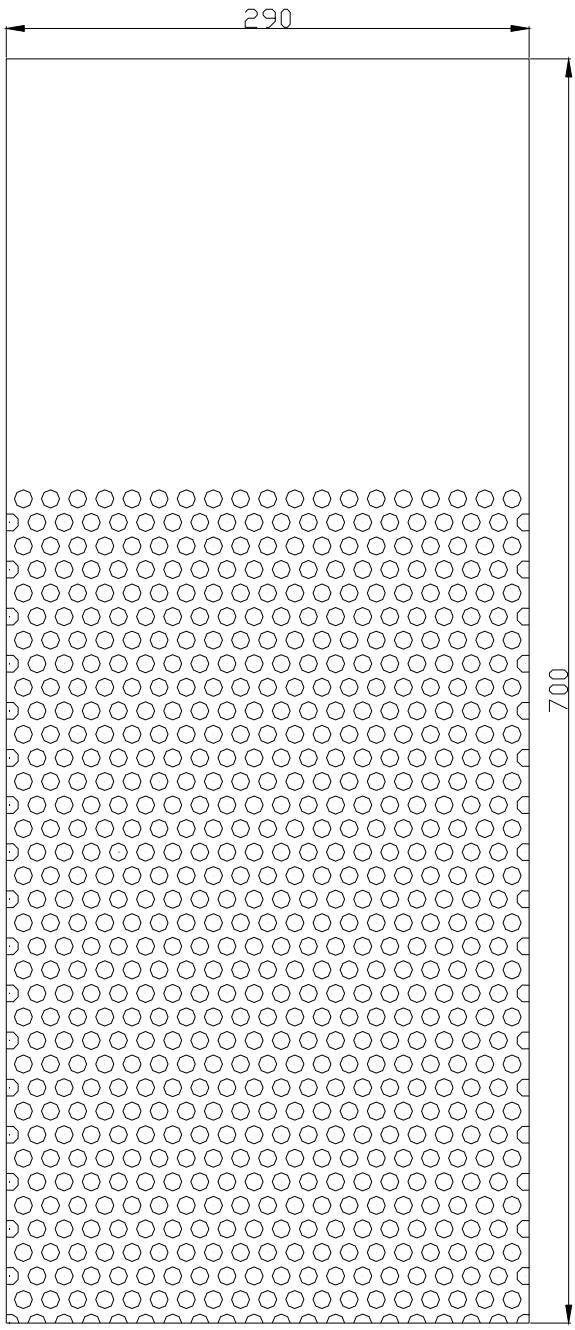

Figure 4.4 Screen with a porosity of 40%

4.2 Experimental Procedure

X/d, t/d and θ, are the major parameters, which were specified at the dimensional analysis stage. In the beginning of the laboratory experiments, the values, which will be used for these parameters in the experiments, were determined. Next, for each set of experiments all possible combinations of these values were used. Table 4.1 shows the values of those parameters. The sign "+" represents each set of experiments and totally 36 sets of experiments were performed in order to determine the effects of those parameters on the energy dissipation.

Table 4.1 The scope of the experiments

X/d	**t/d (d=2cm)**	**θ=90**	**θ=75**	**θ=60**	**t/d (d=4cm)**	**θ=90**	**θ=75**	**θ=60**
50	**1**	+	+	+	**0.5**	+	+	+
	2	+	+	+	**1**	+	+	+
	2D	+	+	+	**1D**	+	+	+
100	**1**	+	+	+	**0.5**	+	+	+
	2	+	+	+	**1**	+	+	+
	2D	+	+	+	**1D**	+	+	+

Table 4.2 X values and gate openings with respect to X/d values

X (cm)	**d=2 cm**	**d=4 cm**
X/d=50	100	200
X/d=100	200	400

As can be seen from the tables above the gate opening was adjusted to two different values of 2 cm and 4 cm. For the first 18 experiments, the gate opening was adjusted to 2 cm. Next, the thickness of the screen, the location of the screen and the inclination of the screen were prepared according to the selected experiment set.

After these system adjustments, the water was released into the pressurized tank by opening the valve and water entered the channel from the gate at the bottom of the pressurized tank. By adjusting the valve, the maximum possible discharge was obtained, at which the water did not exceed the porous section of the screen, and also it was possible to take water depth measurements at pre-selected locations. After the maximum discharge was obtained, the air was extracted from the pressurized tank with the air release valve on the tank. Then differential pressure head readings were taken by using the manometer of the orifice meter. Discharge was obtained indirectly from these readings later at the computation stage. Then, the points G, A and C were determined by observation and the water depths were measured at those points by the mobile point gage. Depth measurements were taken at three different points along the width of the channel, one 5 cm away from the right edge, one at the center and one 5 cm from the left edge. The average of these three water depth values was used for the computation of the energy loss. After the measurements for the maximum discharge were taken, the valve opening was reduced in order to reach the minimum discharge possible, at which no choking occurred and water depth measurements were conveniently performed in the same manner.

Again, for discharge computations differential pressure readings were taken with the manometer of the orifice meter. The water levels were measured by the mobile point gage again at the points G, A and C. Then, other discharges were set and all readings were retaken for each discharge.

All these steps constituted one set of experiment. For the next set, all parameters were kept unchanged (thickness of the screen and height of the gate opening) except for the inclination of the screen. All steps that form a set were repeated for the new inclination angle.

After all the inclination angles were tested at the same place, the location of the screen was changed and the similar procedure was applied at the new location. Finally, the height of the gate was adjusted to the next position and all these combinations were repeated for the new gate opening.

CHAPTER V

RESULTS AND DISCUSSIONS

5.1 Introduction

The results and discussions of the experiments are presented in this Chapter. The reference key for the description of the experiments is described in Table 5.1.

Table 5.1 Reference key

Reference	θ (degree)	t/d	X/d	Fr_G
60-0.5-100-9.78	60	0.5	100	9.78
90-1D-100-11.15	90	1 (double)	100	11.15

5.2 Performance of the system

As previously stated the total energy loss between just downstream of the gate (i.e. point G) and just downstream of the screen (i.e. point C) is denoted as ΔE_{GC}. This energy loss includes the friction losses, losses due to a pseudo-jump or real jump and the screen loss. The system performance is defined by the relative energy loss $\Delta E_{GC}/E_G$. The system performance is influenced by several important parameters such as the inclination angle of the screen, θ; relative screen thickness, t/d; and relative screen position, X/d. In the following sections, the effects of those parameters on the system performance will be presented

.

5.2.1 Effects of inclination angle on the system performance

The main goal of the present study is to determine the effects of inclination of the screens on the energy dissipation. To show those effects Figures 5.1 through 5.7 were selected.

Figure 5.1 shows the effect of inclination of the single and double screens for the inclination angles of 60º, 75º and 90º at the relative screen position of X/d=100. Needless to say that all of the screen configurations dissipate the energy more than a classical full jump does, whose performance is indicated by a solid curved line in the figures. Although not very substantially, it may be discerned from the Figure that as the inclination angle gets smaller the performance of the system slightly improves.

Figures 5.2 and 5.3 show the system performance for single screens for all of the inclinations at X/d=50 and X/d=100, respectively. Likewise, Figures 5.4 and 5.5 show the similar information for double screens. Figures 5.6 and 5.7 include all of the experimental data for both single and double screens at X/d=50 and X/d=100, respectively. Based on Figures 5.1 through 5.7 it may be said that there is a weak dependence of the system performance on the screen inclination. In addition, in all of the Figures, there is a general trend that as the Froude number increases, the system performance, namely $\Delta E_{GC}/E_G$ ratio also increases for all inclination angles.

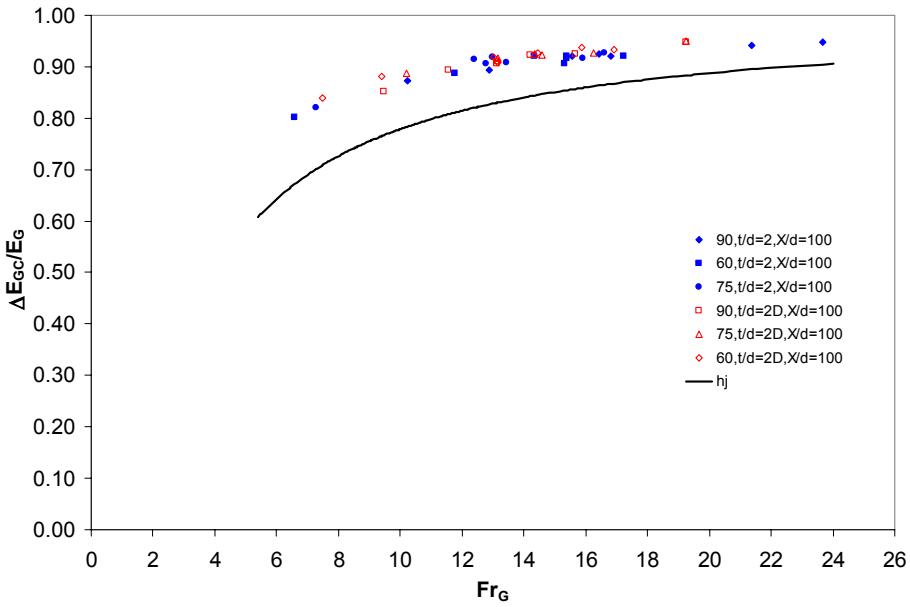

Figure 5.1 $\Delta E_{GC}/E_G$ vs. Fr_G ,the effect of inclination of the single and double screens

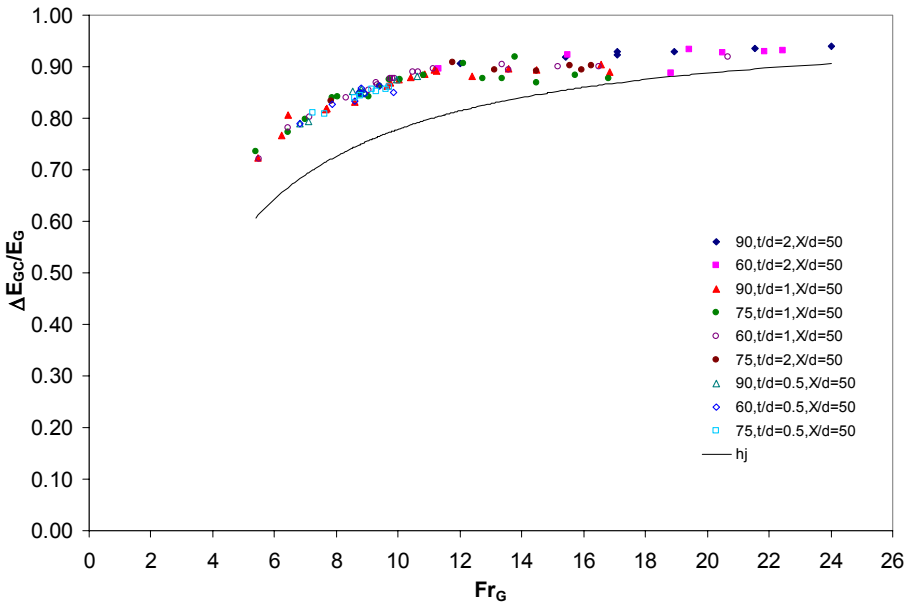

Figure 5.2 $\Delta E_{GC}/E_G$ vs. Fr_G for single screens at X/d=50

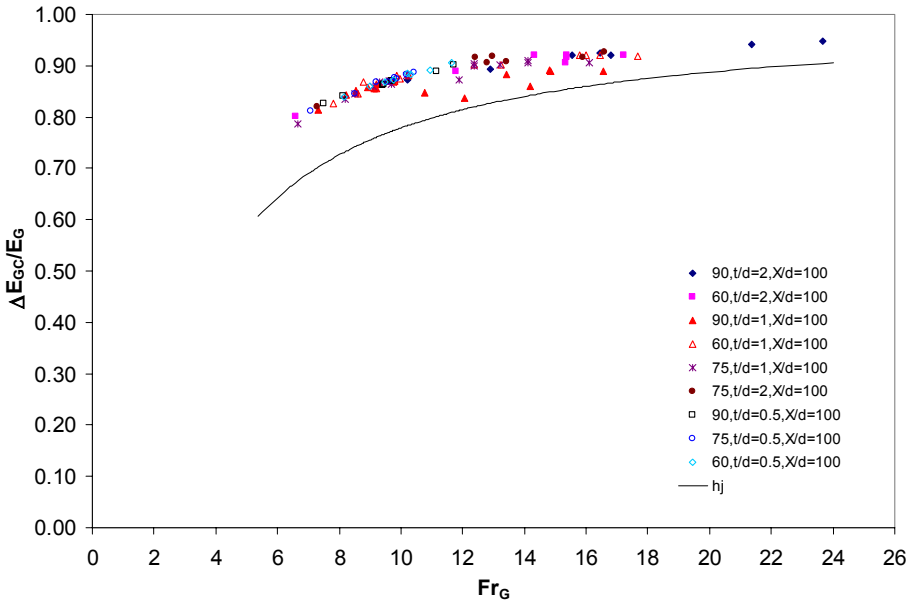

Figure 5.3 $\Delta E_{GC}/E_G$ vs. Fr_G for single screens at X/d=100

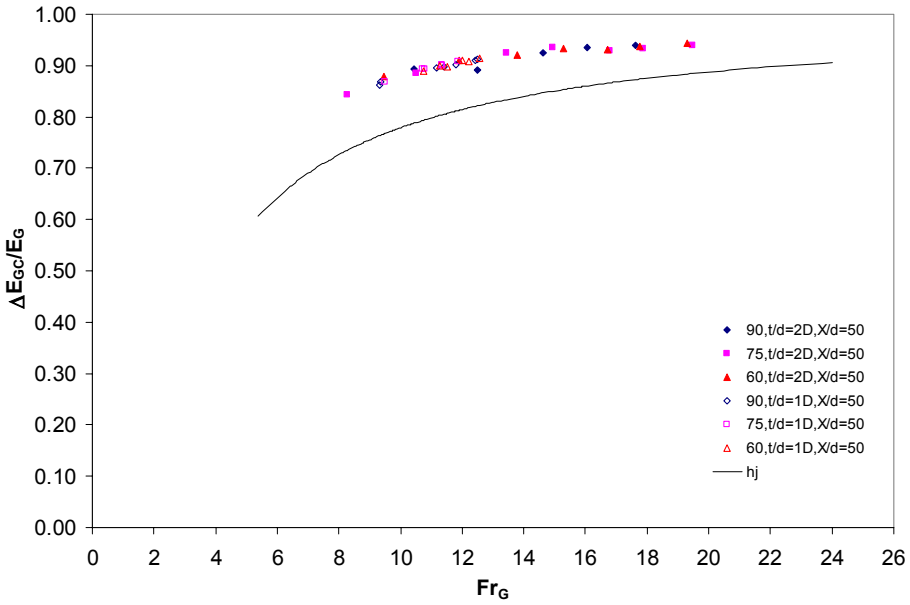

Figure 5.4 $\Delta E_{GC}/E_G$ vs. Fr_G for double screens at X/d=50

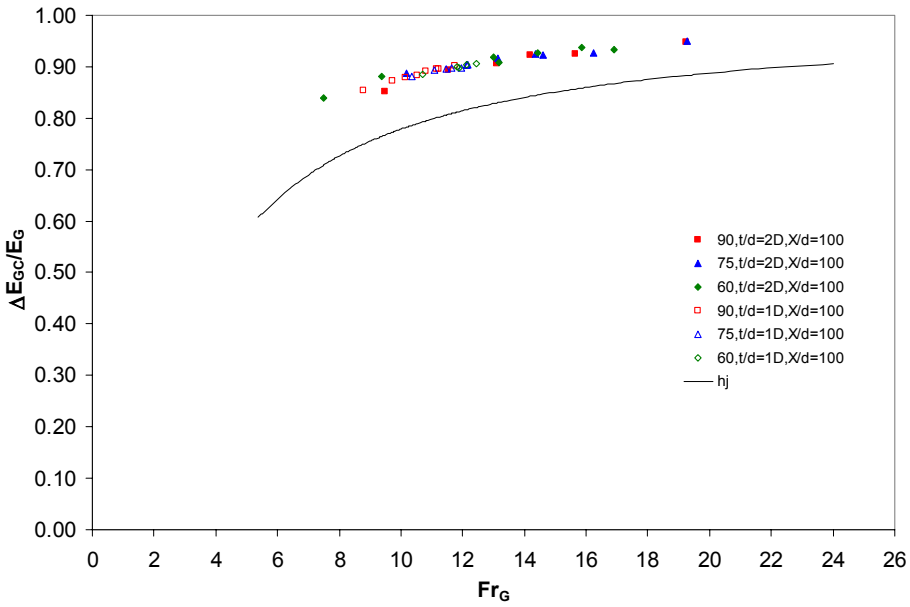

Figure 5.5 $\Delta E_{GC}/E_G$ vs. Fr_G for double screens at X/d=100

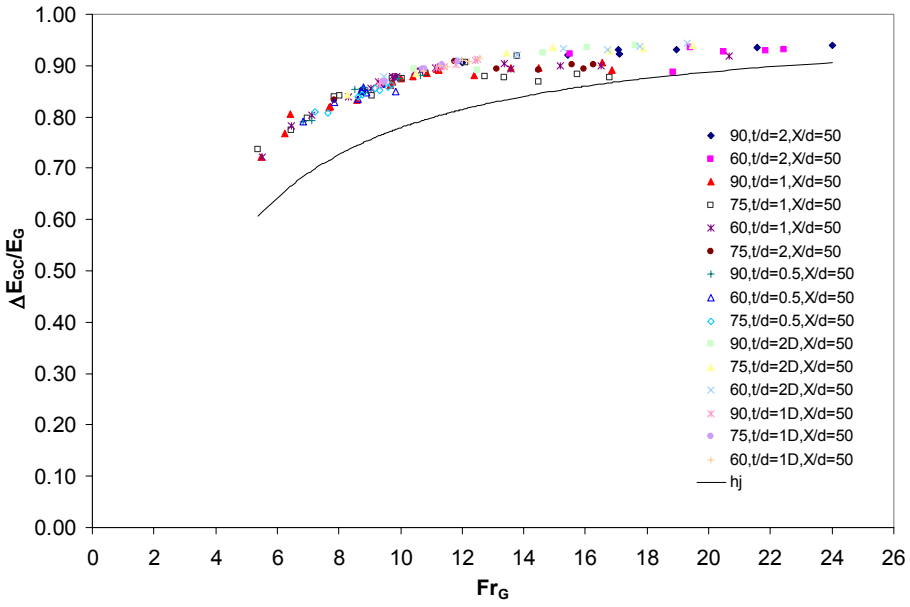

Figure 5.6 $\Delta E_{GC}/E_G$ vs. Fr_G for single and double screens at X/d=50

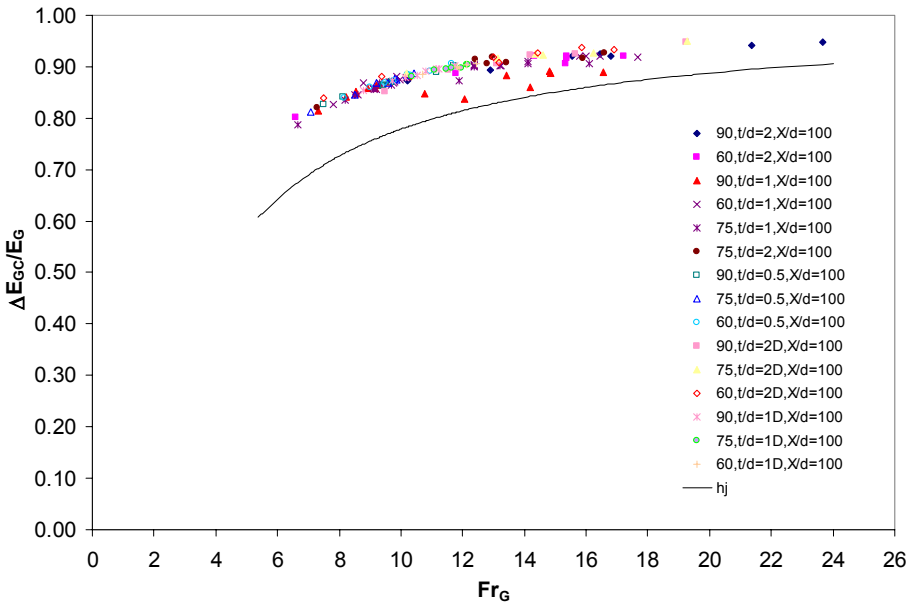

Figure 5.7 $\Delta E_{GC}/E_G$ vs. Fr_G for single and double screens at X/d=100

5.2.2 Effects of relative thickness of the screens on the system performance

Figures 5.8 through 5.13 show the effects of *t/d* values on the system performance for *X/d*=100 and *X/d*=50. In each figure, both single and double screens are included. It is observed in all of the figures that as the relative screen thickness increases the system performance slightly increases for a given Froude number. Again, in all of the figures, the energy dissipation performance of a classical hydraulic jump is shown by a solid curved line.

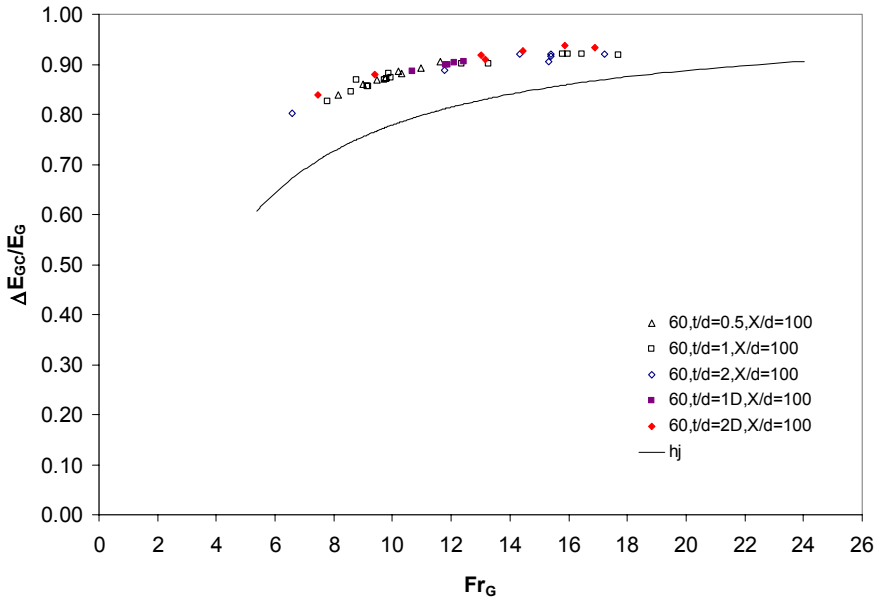

Figure 5.8 $\Delta E_{GC}/E_G$ vs. Fr_G for θ=60 at X/d=100

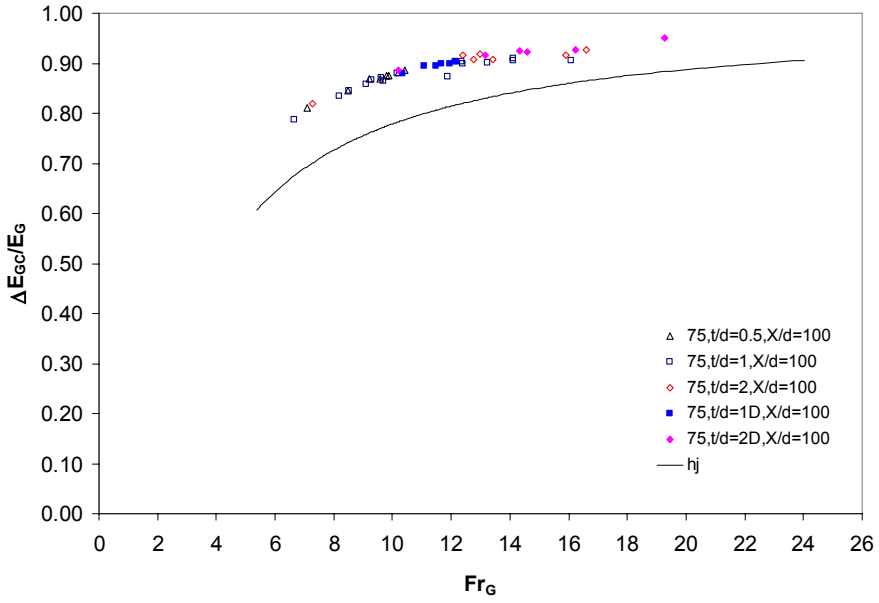

Figure 5.9 $\Delta E_{GC}/E_G$ vs. Fr_G for θ=75 at X/d=100

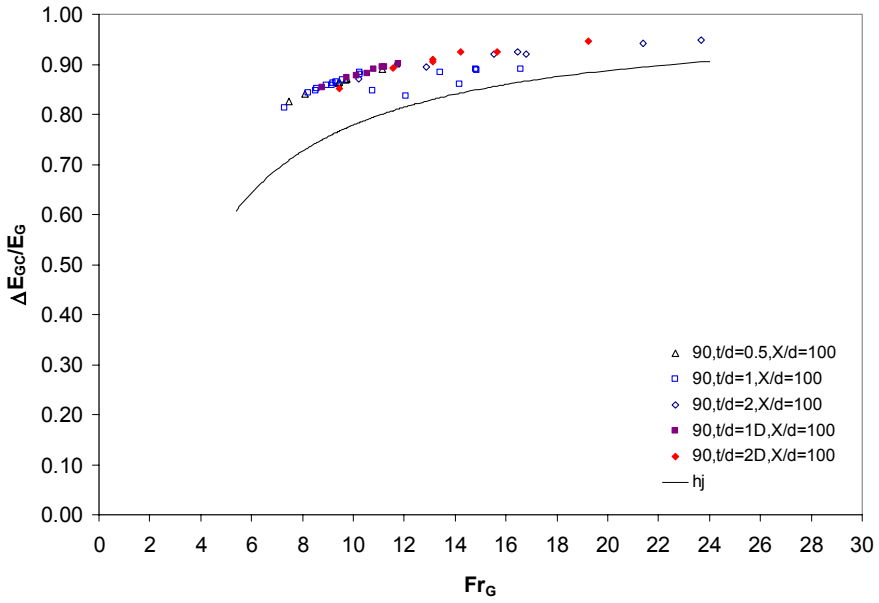

Figure 5.10 $\Delta E_{GC}/E_G$ vs. Fr_G for θ=90 at X/d=100

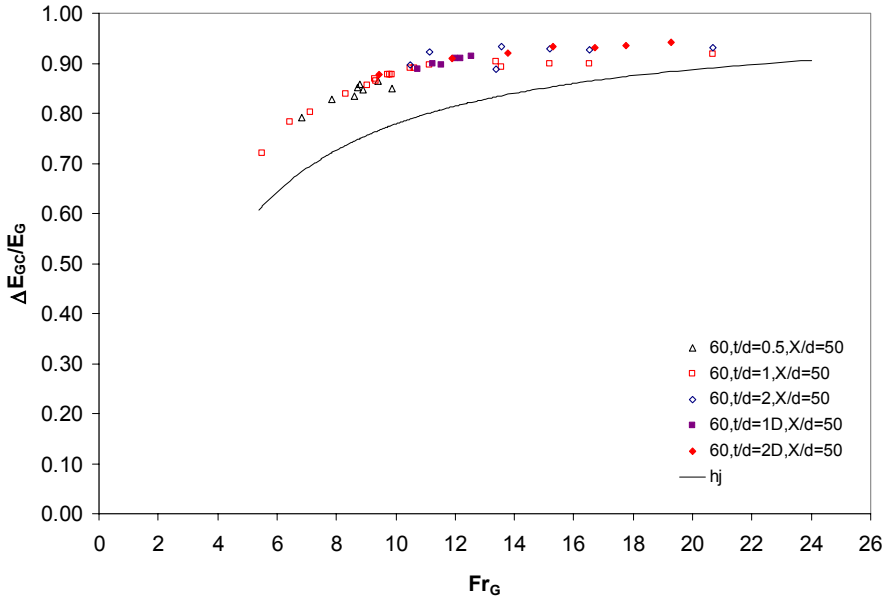

Figure 5.11 $\Delta E_{GC}/E_G$ vs. Fr_G for θ=60 at X/d=50

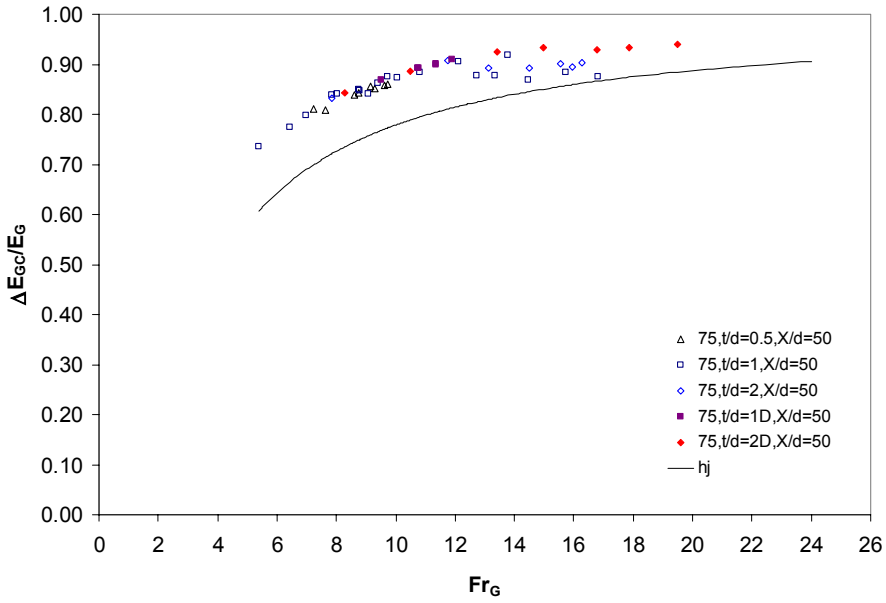

Figure 5.12 $\Delta E_{GC}/E_G$ vs. Fr_G for θ=75 at X/d=50

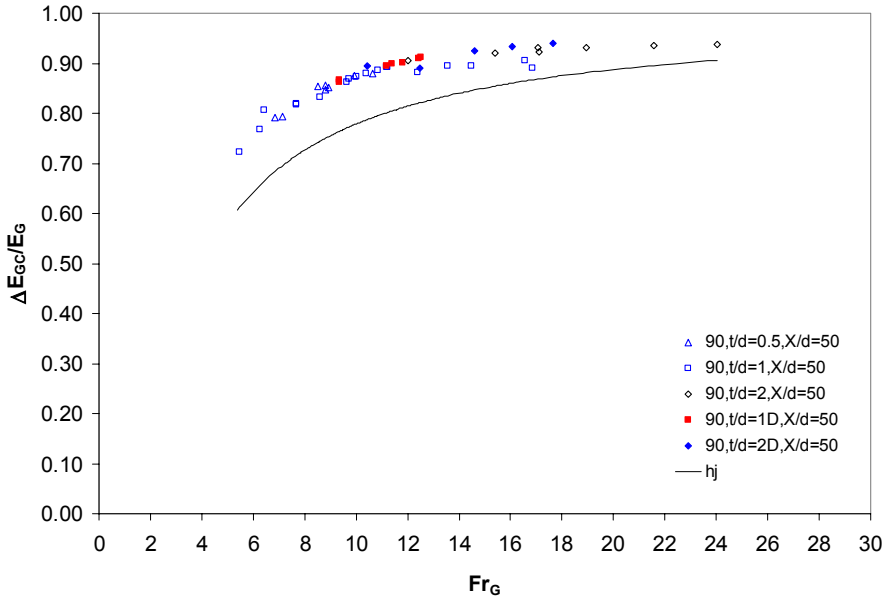

Figure 5.13 $\Delta E_{GC}/E_G$ vs. Fr_G for θ=90 at X/d=50

5.2.3 Effects of relative screen position on the system performance

Figures 5.14, 5.15 and 5.16 show the effect of *X/d* on the system performance for single screens at the inclination angles of θ=60º, θ=75º and θ=90º respectively. Likewise, Figures 5.17, 5.18 and 5.19 give the similar information for double screens. Based on the figures, it may be stated that for the *X/d* values in the range studied (i.e. 50-100) the relative screen position has an insignificant effect on the system performance.

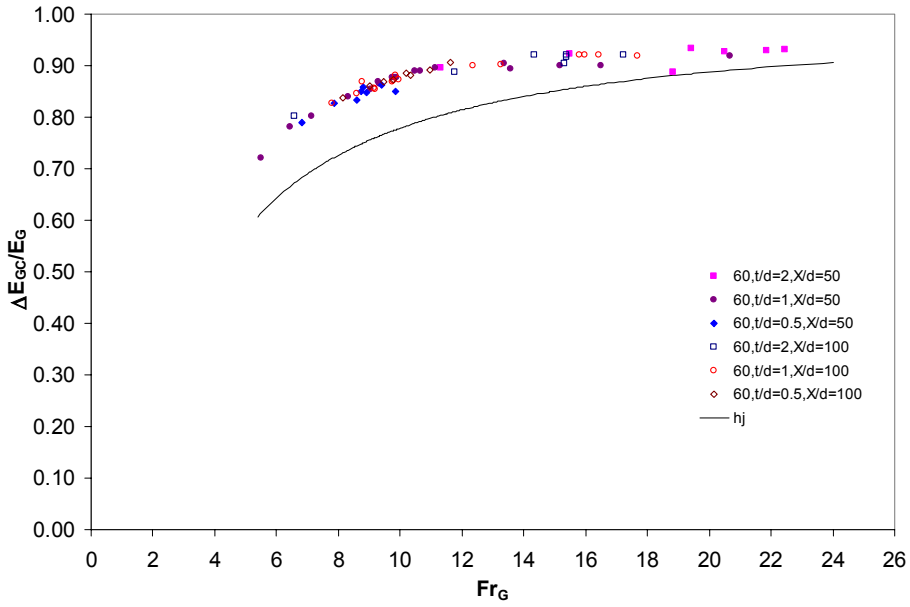

Figure 5.14 $\Delta E_{GC}/E_G$ vs. Fr_G for single screens and θ=60

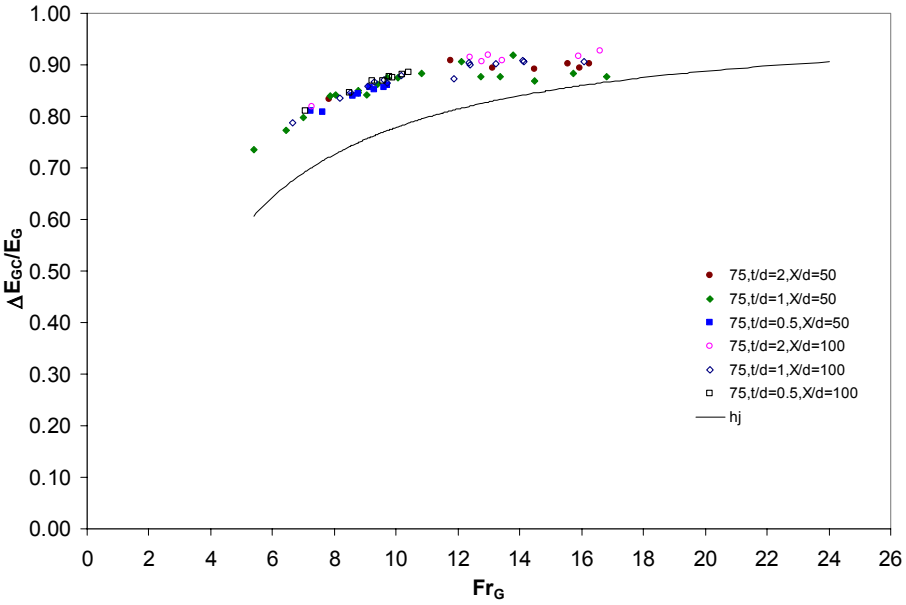

Figure 5.15 $\Delta E_{GC}/E_G$ vs. Fr_G for single screens and θ=75

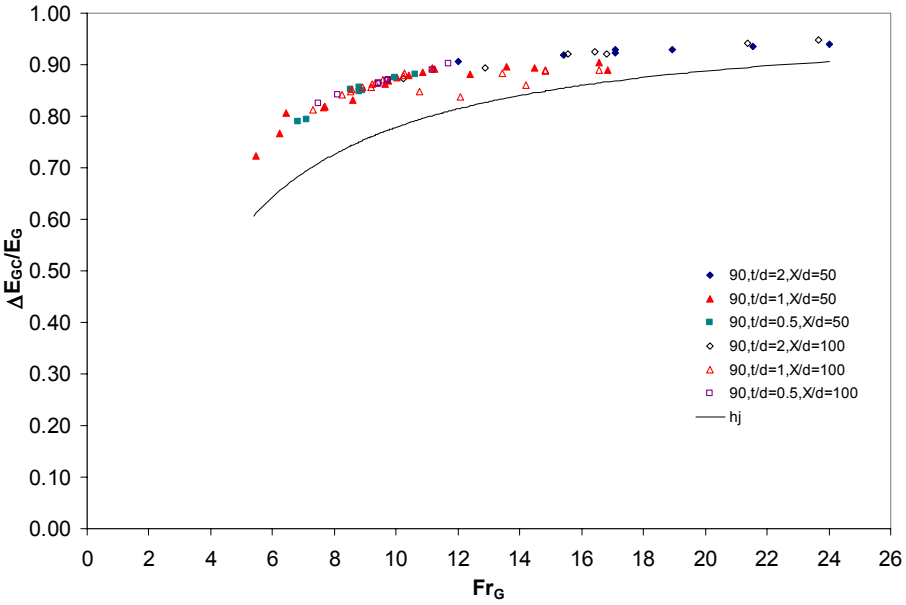

Figure 5.16 $\Delta E_{GC}/E_G$ vs. Fr_G for single screens and θ=90

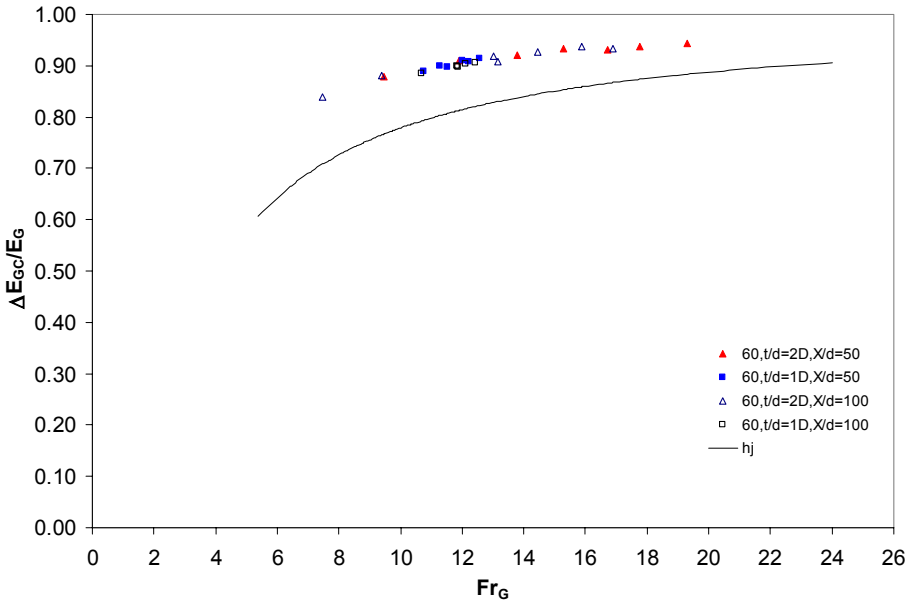

Figure 5.17 $\Delta E_{GC}/E_G$ vs. Fr_G for double screens and θ=60

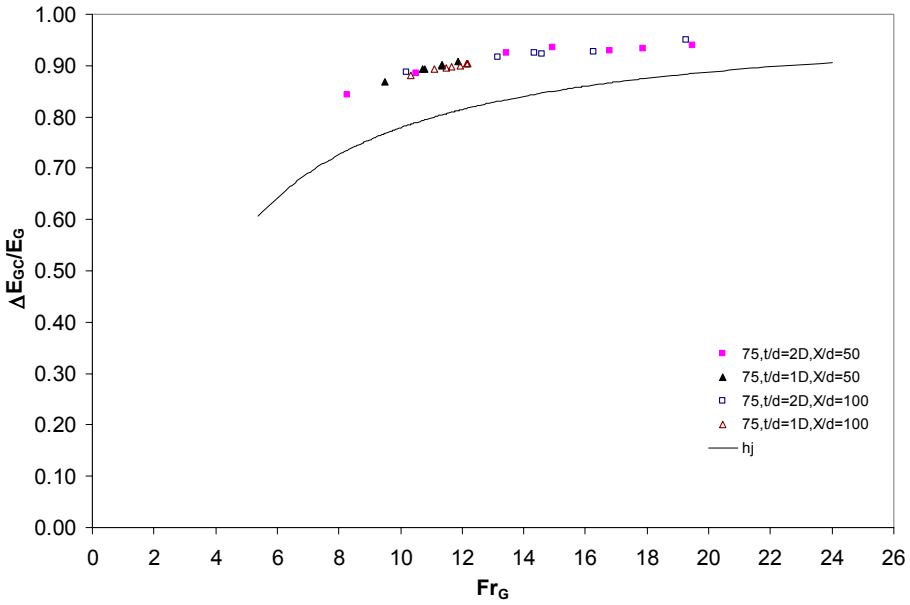

Figure 5.18 $\Delta E_{GC}/E_G$ vs. Fr_G for double screens and θ=75

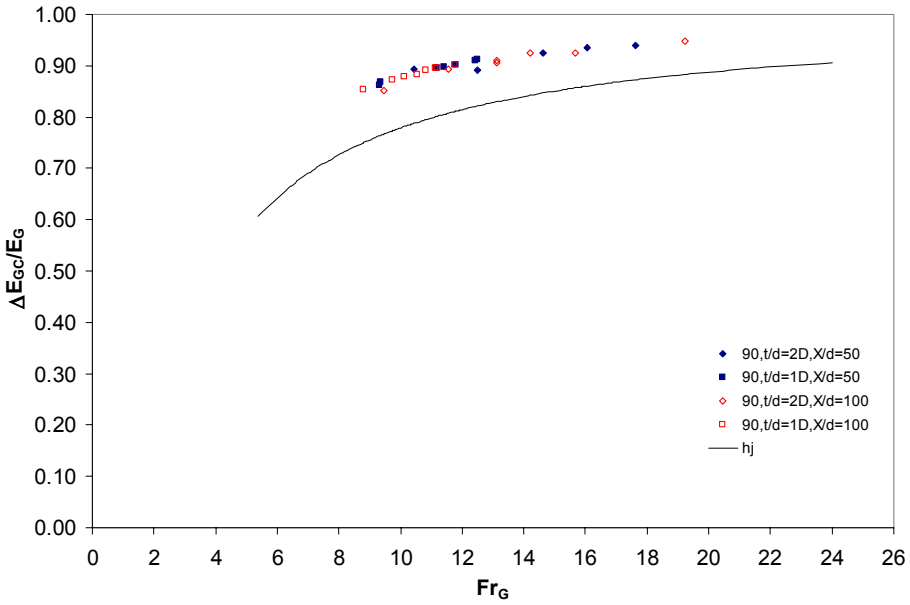

Figure 5.19 $\Delta E_{GC}/E_G$ vs. Fr_G for double screens and θ=90

5.2.4 Comparison of the Present data with that of Çakır, Rajaratnam and Hurtig

Figures 5.20 and 5.21 show the comparison of the system performance between the present study and Çakır's study (2003) for single and double screens, respectively. It should be kept in mind that Çakır studied vertical screens only. The general trend of the data from both of the studies exhibit similarity somewhat. Figure 5.22 is provided to show all data available from Çakır; Rajaratnam and Hurtig and the present study to compare the system efficiency. The range of Froude number in Rajaratnam and Hurtig's data unfortunately do not correspond to the range of the other two studies. However, it still meets the expectation that the system performance should get lower for small Froude numbers.

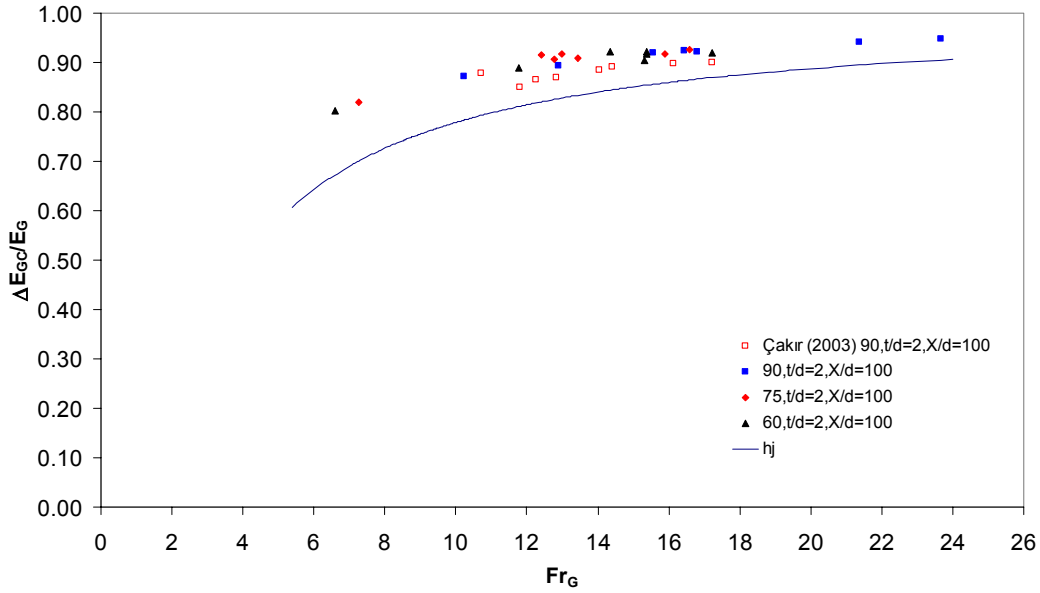

Figure 5.20 Comparison of Çakır's data with that of present work for single screens

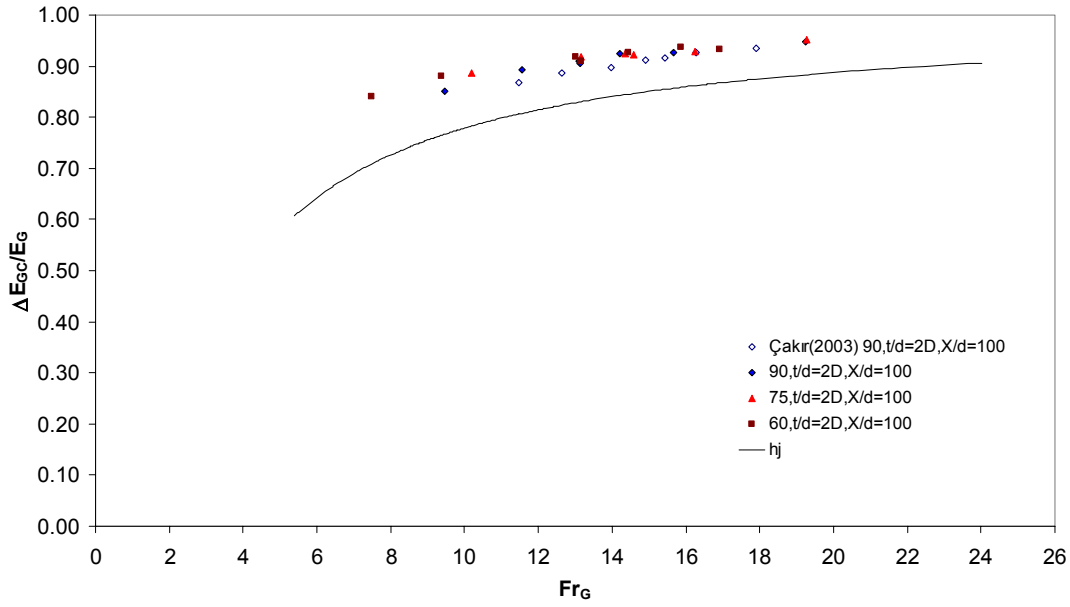

Figure 5.21 Comparison of Çakır's data with that of present work for double screens

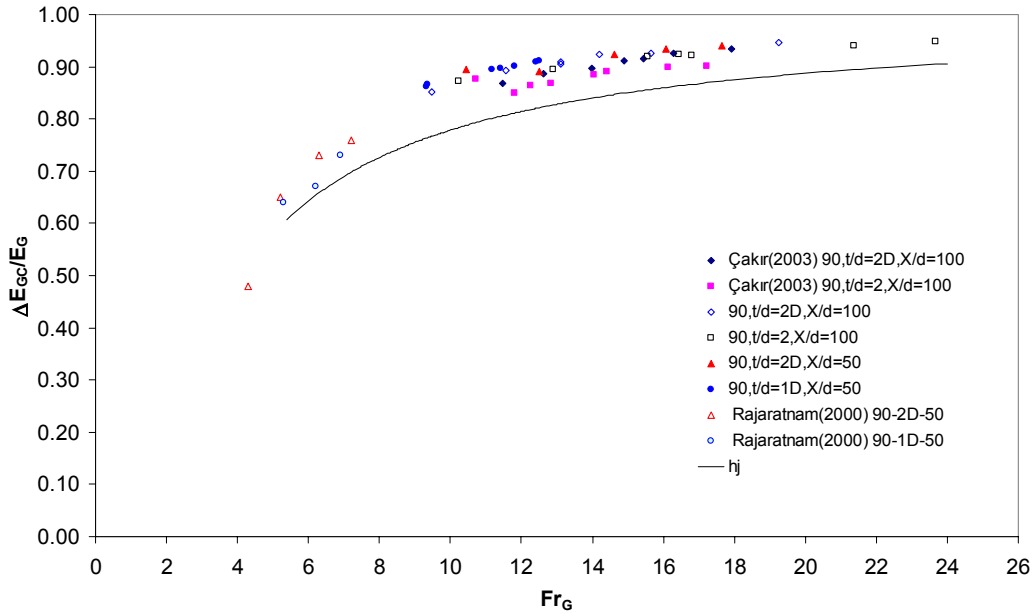

Figure 5.22 Comparison of Çakır's and Rajaratnam and Hurtig's data with that of present work

5.3 Performance of the screen

As previously stated the energy loss at the screen is denoted as S. The screen performance is defined by the relative energy loss S/E_G. The screen performance is influenced by several important parameters such as the inclination angle of the screen, θ; relative screen thickness, t/d; and relative screen position, X/d. In the following sections, the effects of those parameters on the screen performance will be presented.

5.3.1 Effects of inclination angle on the screen performance

Figures 5.23 and 5.24 show the screen performance for single screens for all of the inclinations at X/d=50 and X/d=100, respectively. Similarly, Figures 5.25 and 5.26 show the same information for double screens. Based on Figures 5.23 through 5.26 it can be stated that inclination of the screen has an insignificant effect on the screen performance over the vertical screens. In addition, in Figures 5.23 and 5.25

where *X/d*=50, there is a general trend that as the Froude number increases, the screen performance, namely S/E_G ratio also increases for all inclination angles.

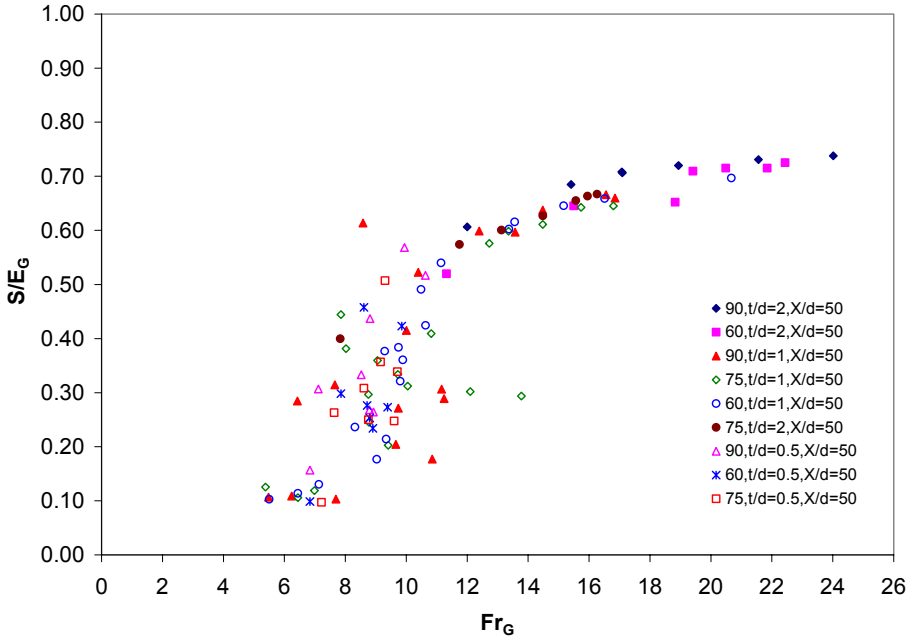

Figure 5.23 S/E_G vs. Fr_G for single screens at X/d=50

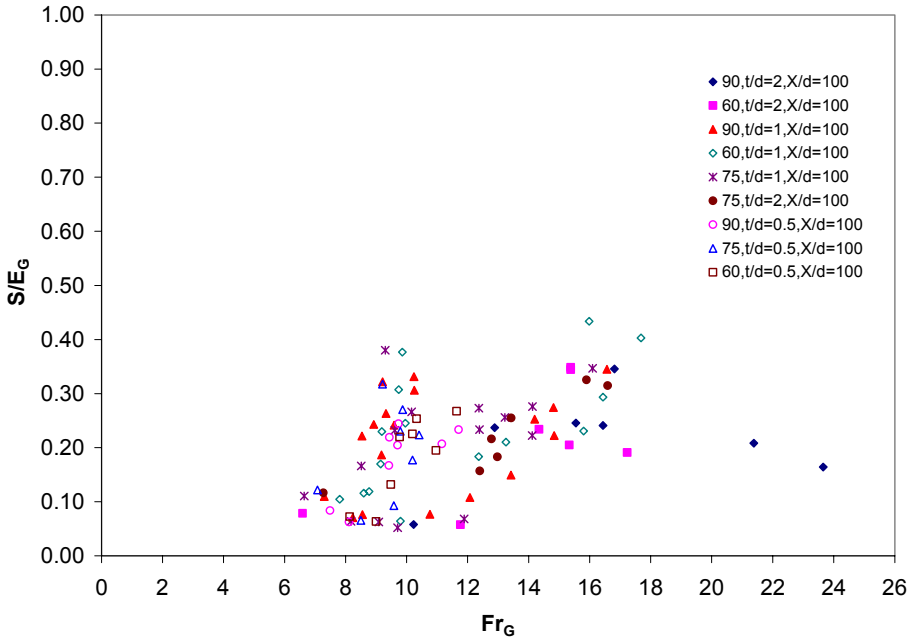

Figure 5.24 S/E_G vs. Fr_G for single screens at X/d=100

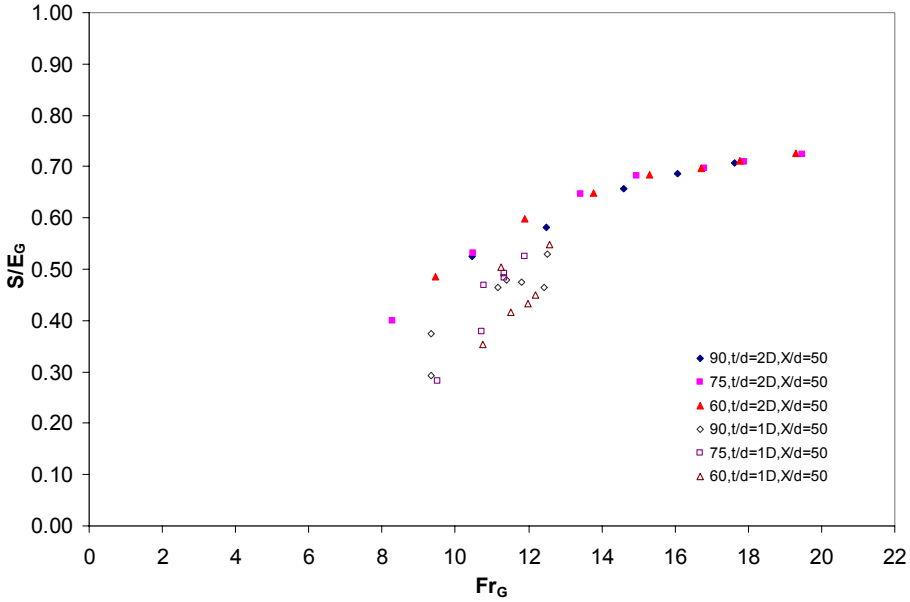

Figure 5.25 S/E_G vs. Fr_G for double screens at X/d=50

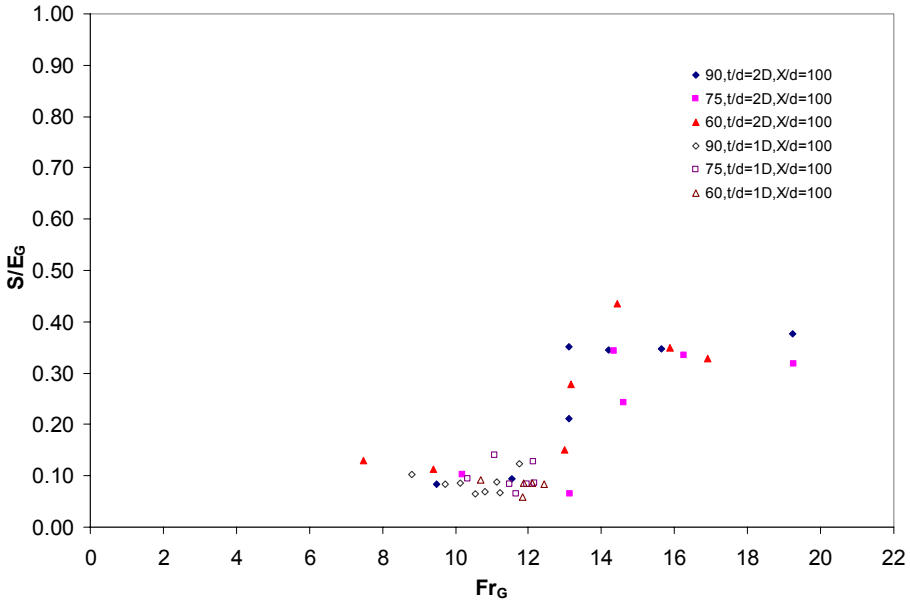

Figure 5.26 S/E_G vs. Fr_G for double screens at X/d=100

5.3.2 Effects of relative thickness of the screens on the screen performance

Figures 5.27 through 5.32 show the effects of *t/d* values on the screen performance for *X/d*=100 and *X/d*=50. In each figure, both single and double screens are included. It is observed in all of the figures that as the relative screen thickness increases the screen performance slightly increases for a given Froude number.

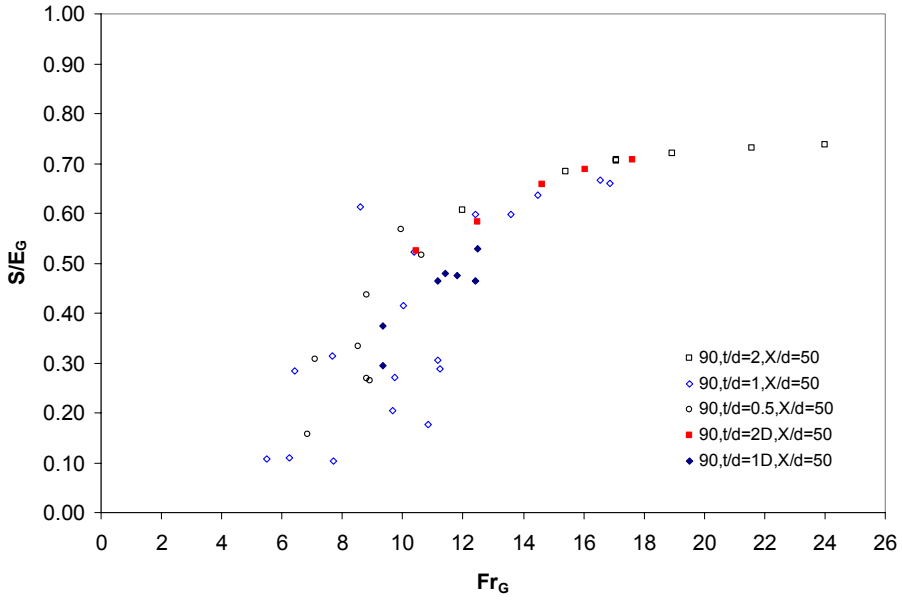

Figure 5.27 S/E_G vs. Fr_G for θ=90 at X/d=50

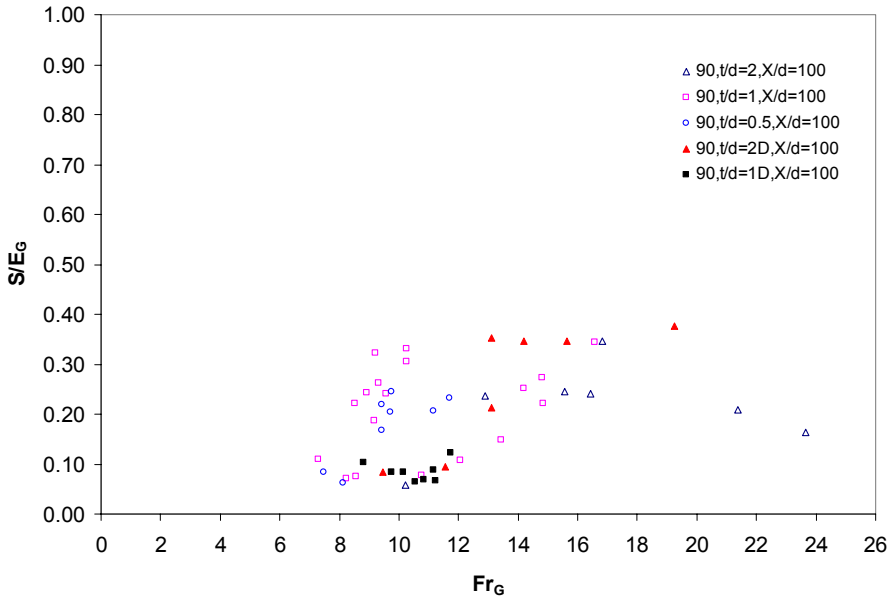

Figure 5.28 S/E_G vs. Fr_G for θ=90 at X/d=100

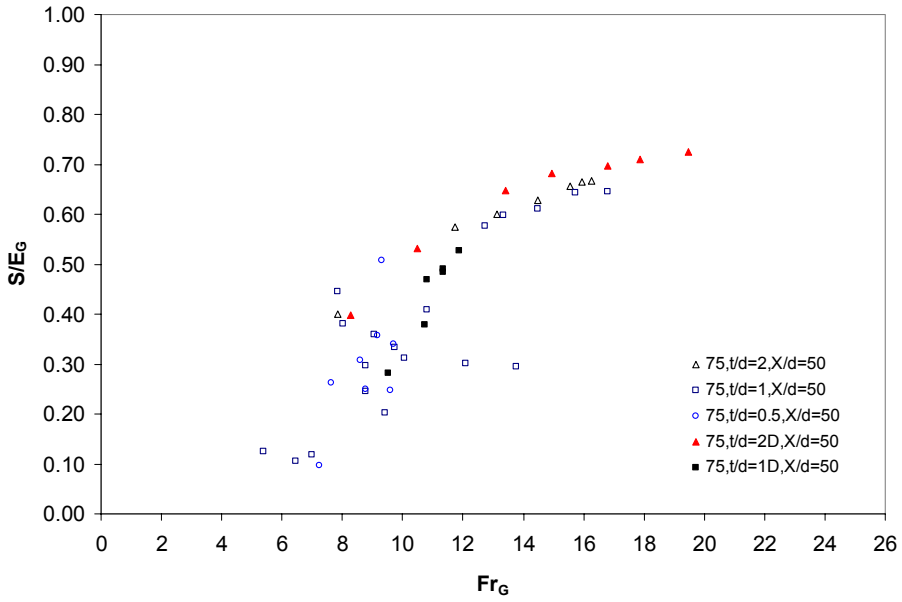

Figure 5.29 S/E_G vs. Fr_G for θ=75 at X/d=50

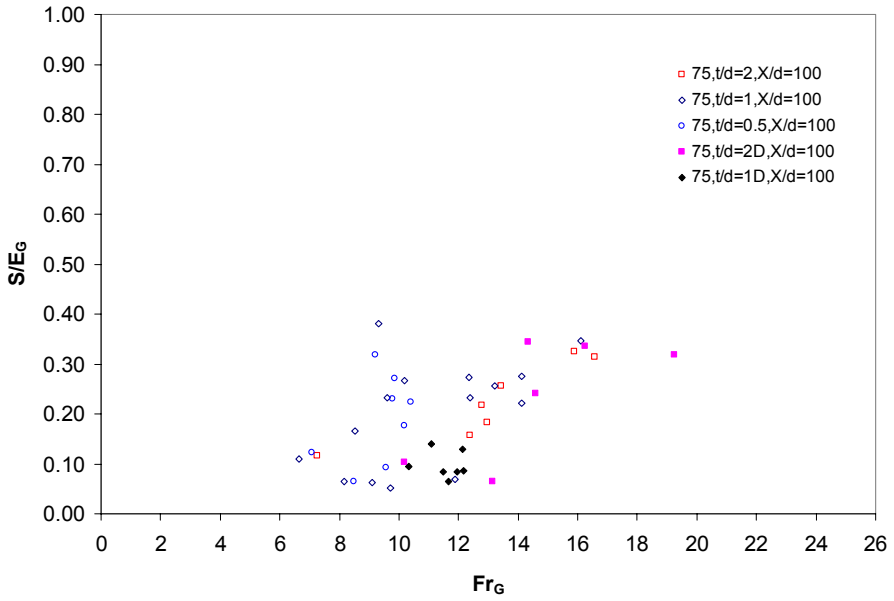

Figure 5.30 S/E_G vs. Fr_G for θ=75 at X/d=100

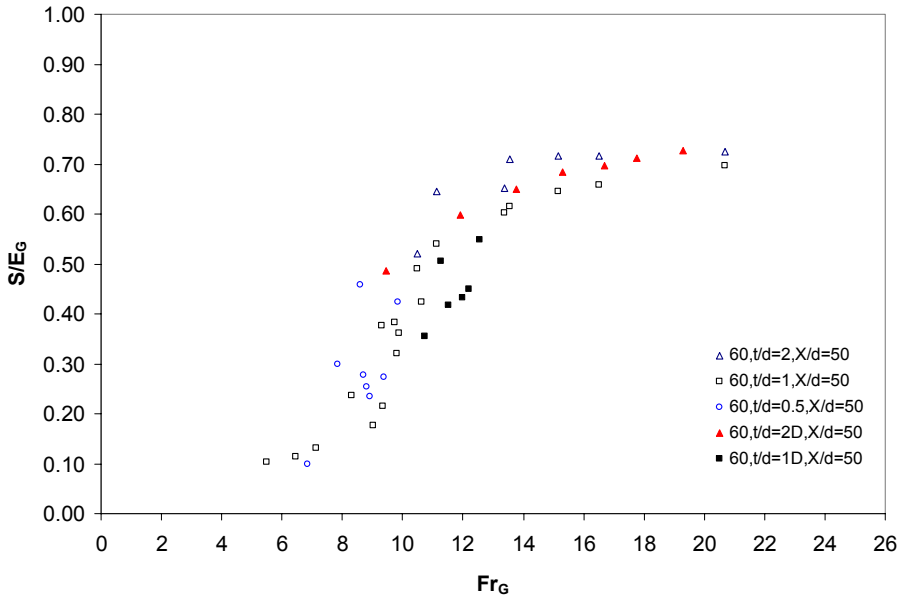

Figure 5.31 S/E_G vs. Fr_G for θ=60 at X/d=50

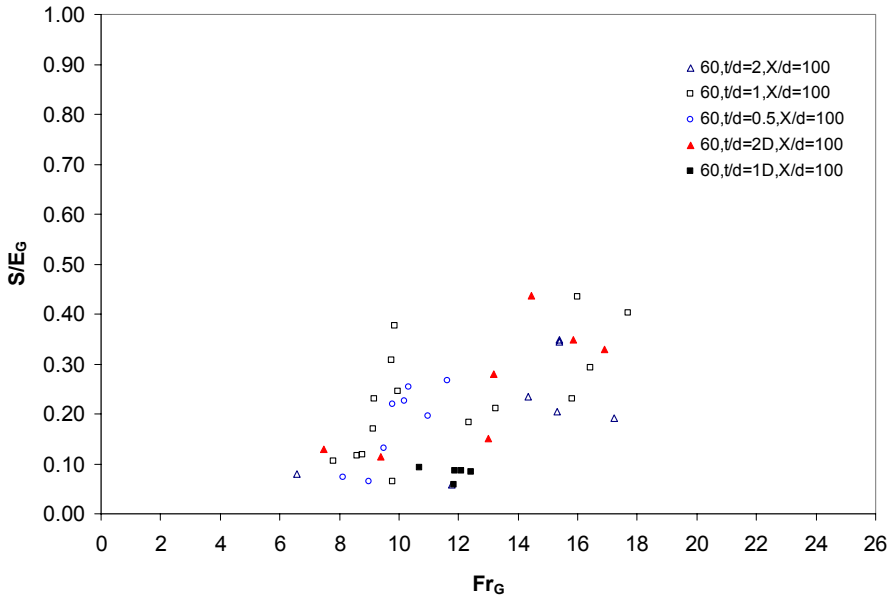

Figure 5.32 S/E_G vs. Fr_G for θ=60 at X/d=100

5.3.3 Effects of relative screen position on the screen performance

Figures 5.33, 5.34 and 5.35 show the effect of *X/d* on the screen performance for single screens at the inclination angles of *θ*=60º, θ=75º and θ=90º respectively. Likewise, Figures 5.36, 5.37 and 5.38 give the similar information for double screens. Based on the figures, it may be stated that for the *X/d* values in the range studied (i.e. 50-100) the relative screen position has an insignificant effect on the screen performance. In addition, there is a general trend for small *X/d* values (i.e. 50), that as the Froude number increases, the screen performance, namely S/E_G ratio also increases for all inclination angles.

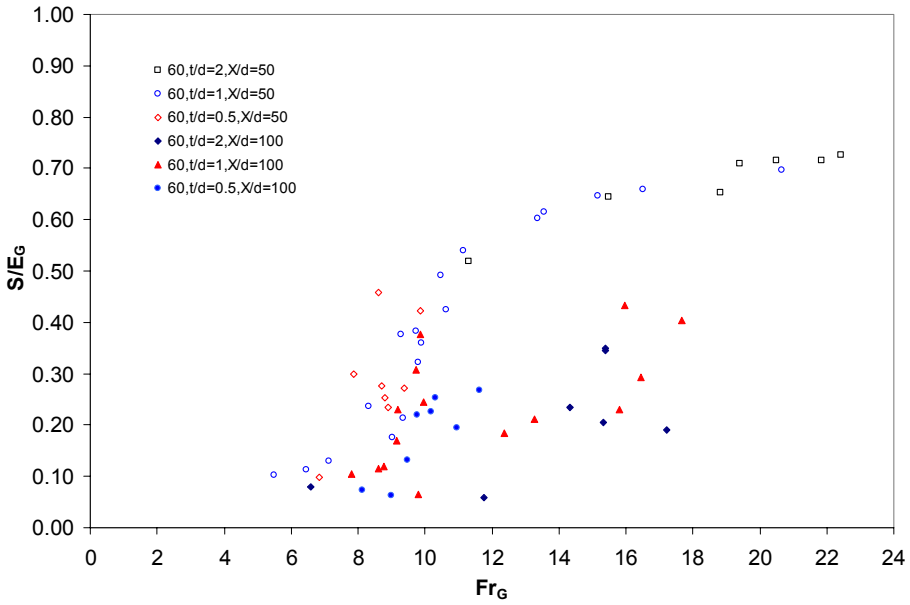

Figure 5.33 S/E_G vs. Fr_G for single screens and θ=60

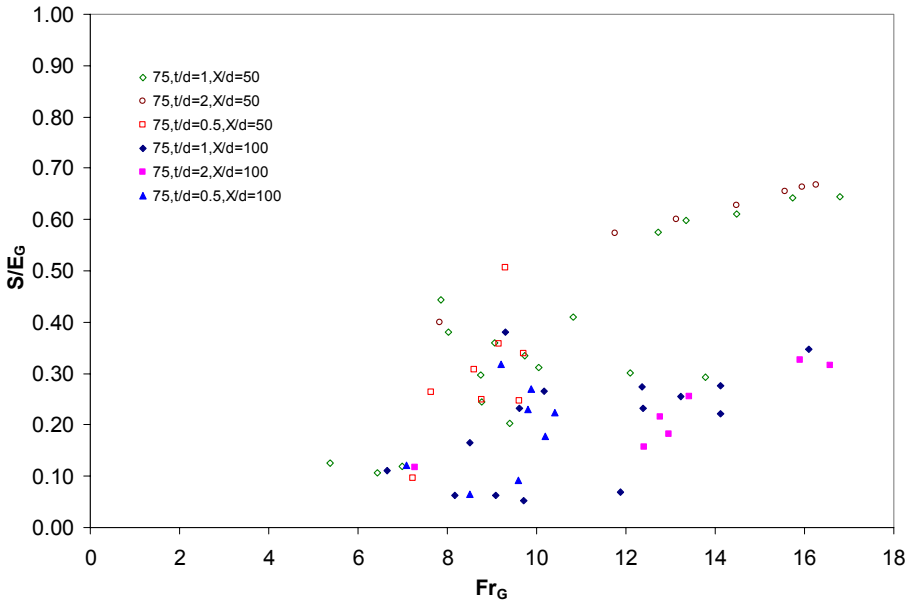

Figure 5.34 S/E_G vs. Fr_G for single screens and θ=75

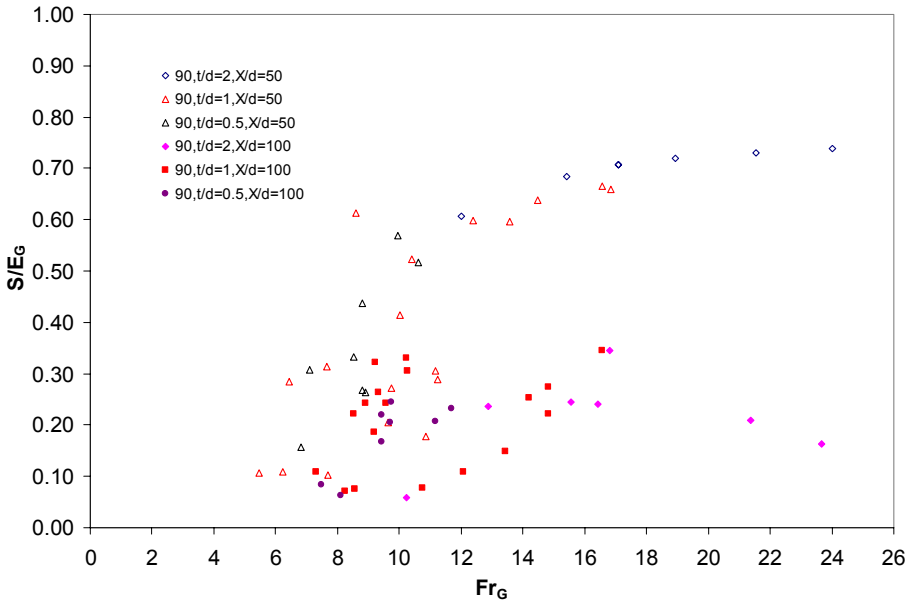

Figure 5.35 S/E_G vs. Fr_G for single screens and θ=90

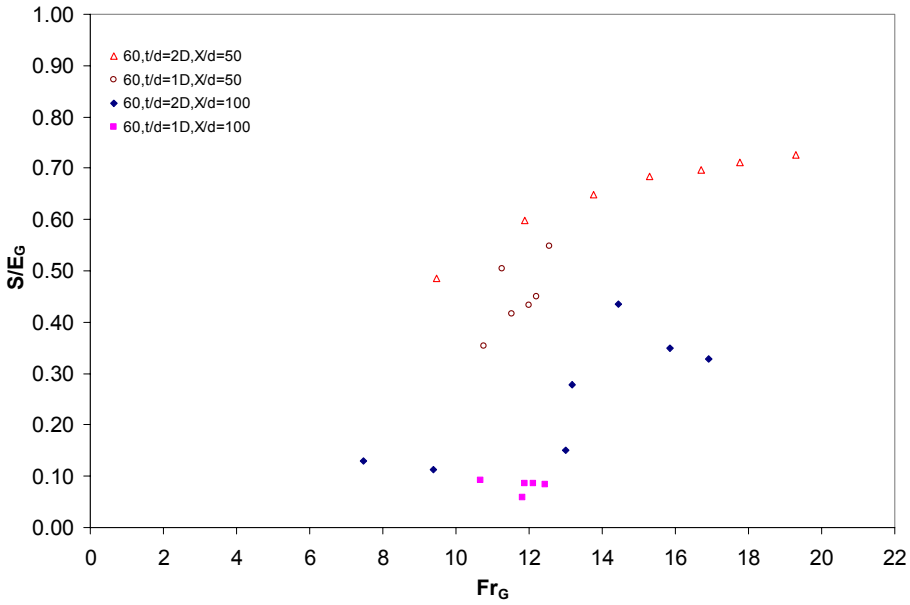

Figure 5.36 S/E_G vs. Fr_G for double screens and θ=60

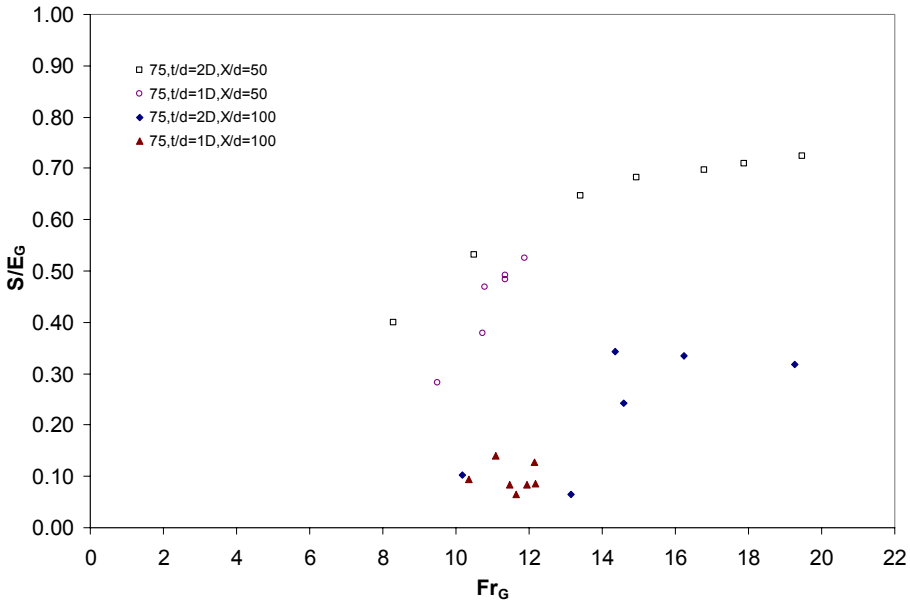

Figure 5.37 S/E_G vs. Fr_G for double screens and θ=75

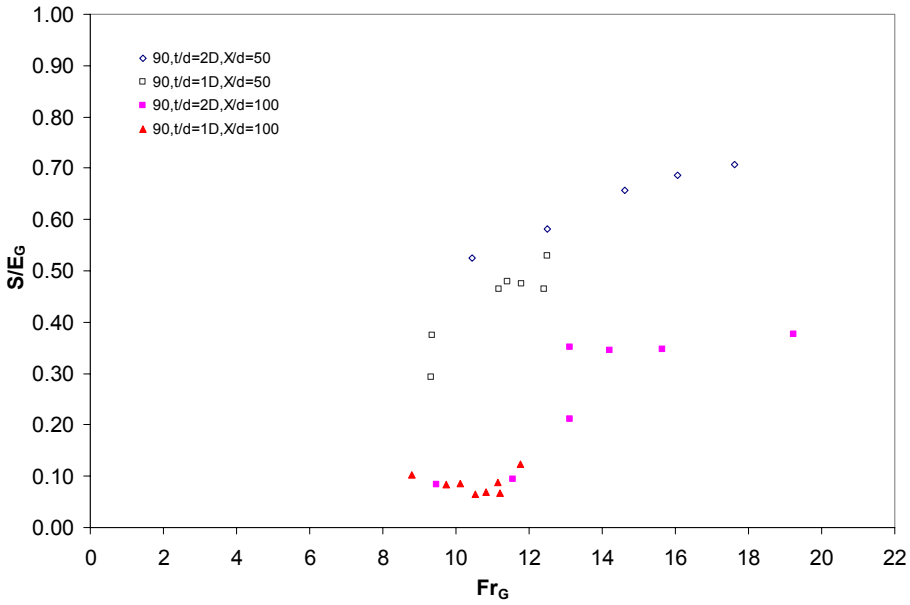

Figure 5.38 S/E_G vs. Fr_G for double screens and θ=90

5.4 System Efficiencies

The system efficiency is defined as follows;

$$\eta_{sys} = \frac{\Delta E_{GC} - \Delta E_{jG}}{\Delta E_{jG}} \tag{5.1}$$

In order to show the effects of the screen inclination, relative thickness of the screen and relative position of the screen on the system efficiency, Figures 5.39 through 5.42 were selected.

At the first glance, it is observed that double screens perform slightly better than single screens for all of the inclination angles.

Figures 5.39 and 5.40 show the system efficiency for single screens for all of the inclinations at *X/d*=50 and *X/d*=100, respectively. Similarly, Figures 5.41 and 5.42 show the same information for double screens. Based on Figures 5.39 through 5.42 it can be stated that inclination of the screen has an insignificant effect on the system efficiency.

In addition, it is observed in all of the figures that as the relative screen thickness increases the system efficiency slightly increases for a given Froude number.

Also, based on the figures, it can be stated that for the *X/d* values in the range studied (i.e. 50-100) the relative screen position has an insignificant effect on the system efficiency.

Lastly, in all of the Figures, there is a general trend that as the Froude number increases, the system efficiency decreases for all inclination angles.

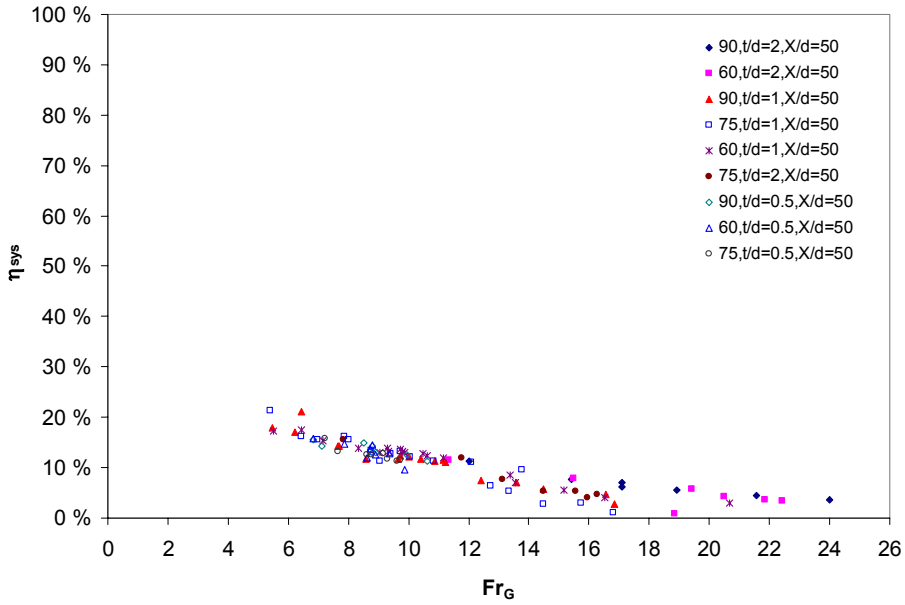

Figure 5.39 η_{sys} vs. Fr_G for single screens at X/d=50

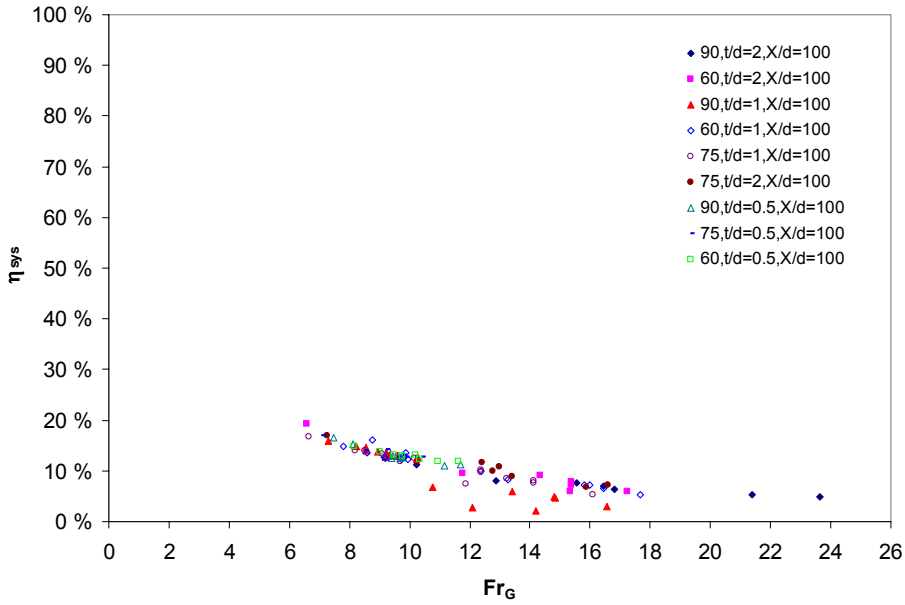

Figure 5.40 η_{sys} vs. Fr_G for single screens at X/d=100

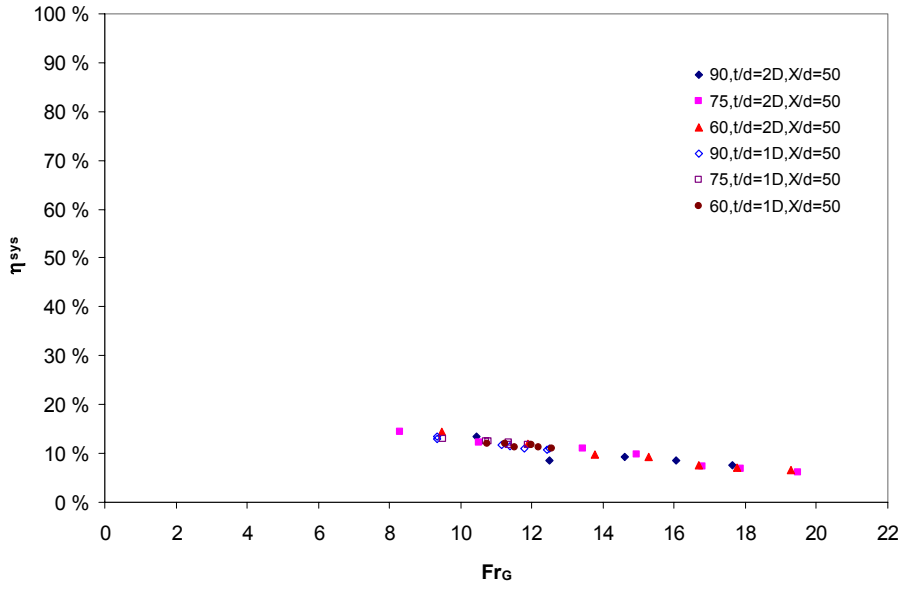

Figure 5.41 η_{sys} vs. Fr_G for double screens at X/d=50

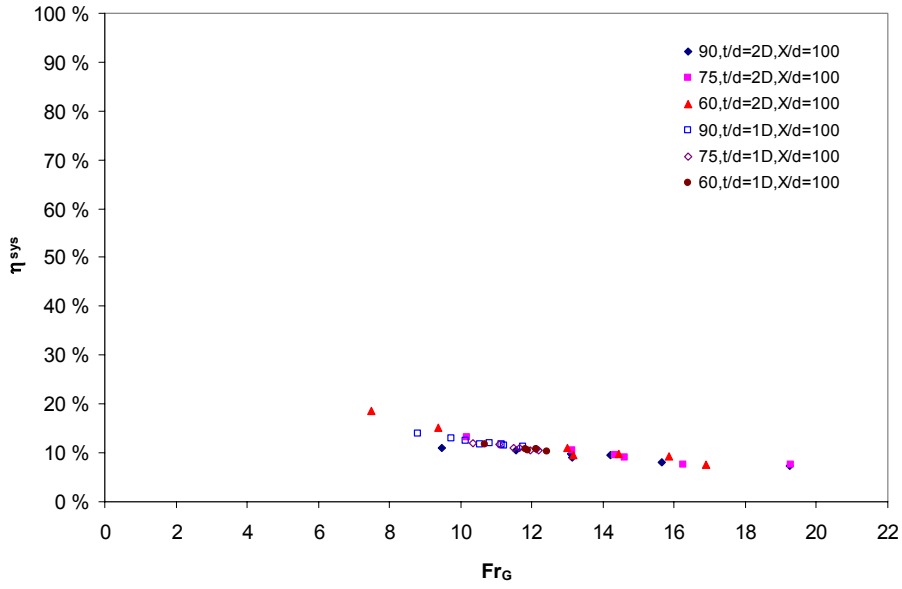

Figure 5.42 η_{sys} vs. Fr_G for double screens at X/d=100

5.5 Screen Efficiencies

Screen efficiency is defined as follows;

$$\eta_{scr} = \frac{S}{\Delta E_{jG}} \tag{5.2}$$

In order to show the effects of the screen inclination, relative thickness of the screen and relative position of the screen on the screen efficiency, Figures 5.43 through 5.46 were selected.

Figures 5.43 and 5.44 show the screen efficiency for single screens for all of the inclinations at *X/d*=50 and *X/d*=100, respectively. Similarly, Figures 5.45 and 5.46 show the same information for double screens. Based on Figures 5.43 through 5.46 it can be stated that inclination of the screen has an insignificant effect on the screen efficiency.

In addition, it is observed in all of the figures that as the relative screen thickness increases for a given Froude number the screen efficiency slightly increases.

Also, based on the figures, it can be stated that for the *X/d* values in the range studied (i.e. 50-100) as the relative screen position increases the screen efficiency decreases for a given Froude number.

Lastly, for small *X/d* values (i.e. 50), there is a general trend that as the Froude number increases, the screen efficiency increases for all inclination angles.

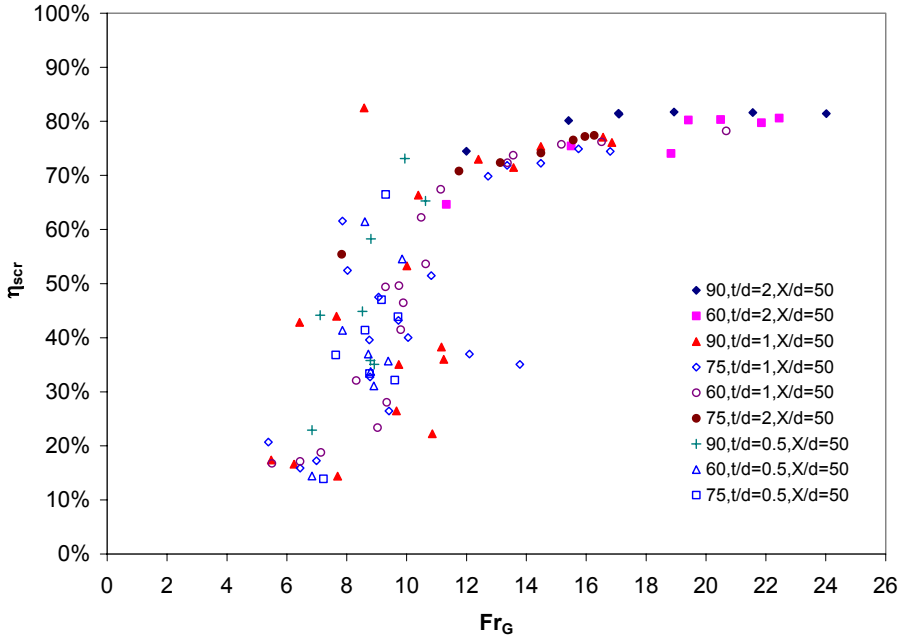

Figure 5.43 η_{scr} vs. Fr_G for single screens at X/d=50

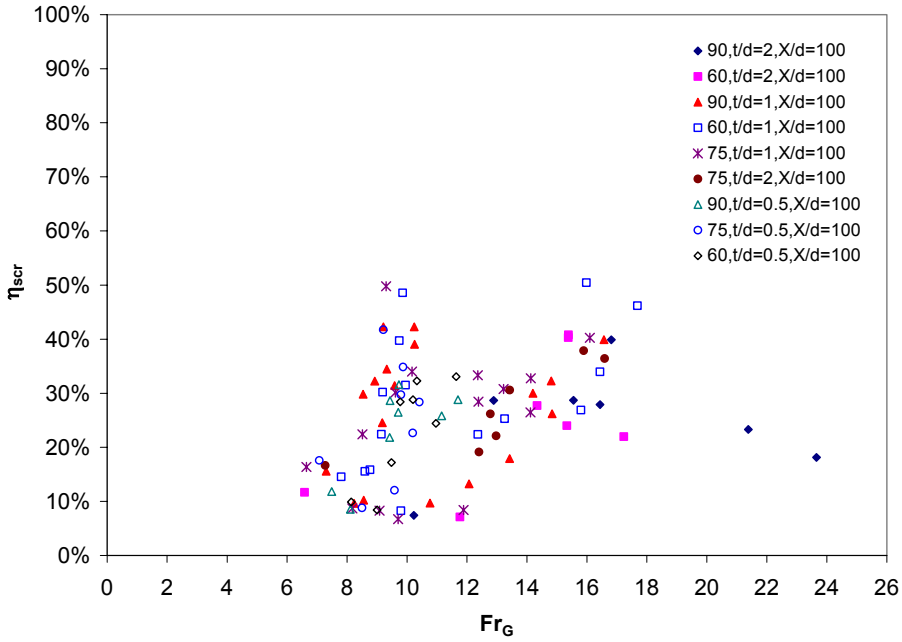

Figure 5.44 η_{scr} vs. Fr_G for single screens at X/d=100

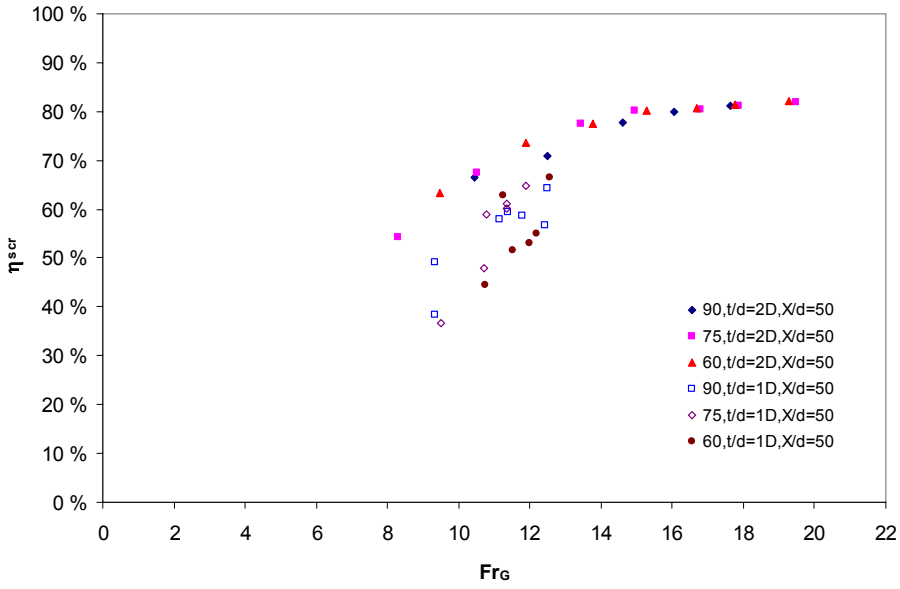

Figure 5.45 η_{scr} vs. Fr_G for double screens at X/d=50

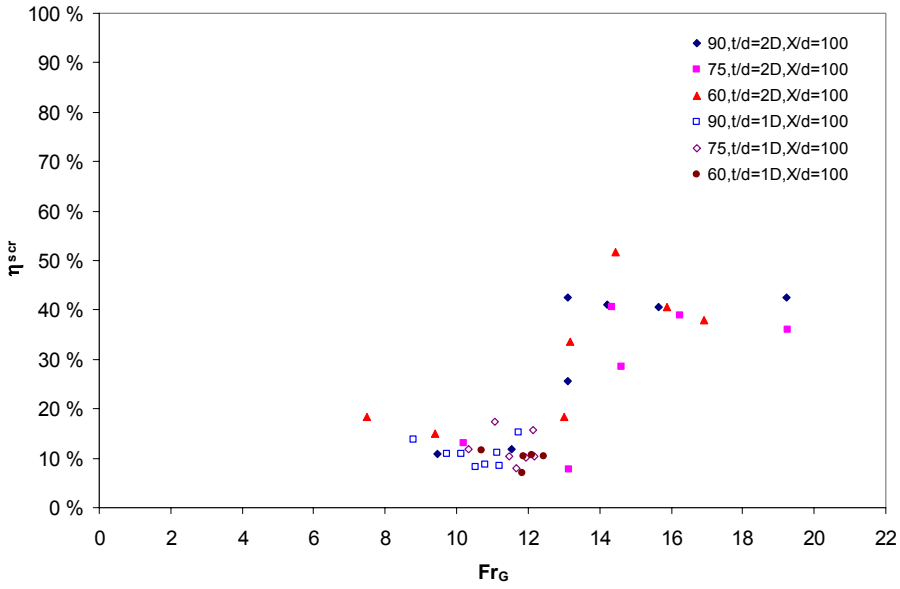

Figure 5.46 η_{scr} vs. Fr_G for double screens at X/d=100

CHAPTER VI

CONCLUSIONS AND RECOMMENDATIONS

In the present study the effects of screen inclination on the energy dissipation performance of the screen were investigated by performing a series of laboratory experiments. As stated in the previous chapters, screens with a porosity of 40% were used for the experiments. Froude numbers of the upstream flow covered a range of 5 to 24 and locations of the screens measured from the gate of the pressurized tank were from 50 times to 100 times of the upstream flow depth. Inclination angle of the screen was chosen as 90˚, 75˚, and 60˚ measured in the vertical plane from the channel bottom upstream of the inclined screens.

Conclusions obtained from the analysis of the experimental data are as follows;

1. All of the screen configurations dissipate the energy more than a classical full jump does,

2. Inclination of the screen has an insignificant effect on the system performance, screen performance, system efficiency and screen efficiency,

3. There is a general trend that as the Froude number increases, the system performance also increases for all inclination angles,

4. As the relative screen thickness increases the system performance, screen performance, system efficiency and screen efficiency slightly increases for a given Froude number,

5. For the *X/d* values in the range studied (i.e. 50-100) the relative screen position has an insignificant effect on the system performance, screen performance and system efficiency,

6. There is a general trend that as the Froude number increases, the system efficiency decreases for all inclination angles,

7. For the *X/d* values in the range studied (i.e. 50-100) as the relative screen position increases the screen efficiency decreases for a given Froude number,

8. For small *X/d* values (i.e. 50), there is a general trend that as the Froude number increases, the screen efficiency, and the screen performance increase for all inclination angles.

Energy dissipation through screens problem can be improved by taking into account the following factors.

- Multiple screens
- Screens with different hole geometry
- Thicker screens
- Triangular screens

For the real life application of the screens as energy dissipaters, accumulation of debris and vibration of screens and their effect on the energy dissipative capability of the screens must be considered.

REFERENCES

Bozkuş, Z., Çakır, P., Ger, M. and Özeren, Y.(2004) "Energy Dissipation Through Screens ", Proceedings of ASCE World Water & Environmental Resources Congress 2004 ,Salt Lake City, Utah, U.S.A.

Çakır, Pınar, (2003). "Experimental Investigation of Energy Dissipation through screens". MSc Thesis Department of Civil Engineering Middle East Technical University, Ankara, Turkey

French, R. H. (1986). "Open Channel Hydraulics." McGraw-Hill Book Company, Singapore.

Munson, B.R., Young, D. F. and Okiishi, T. H. (1994). "Fundamentals of Fluid Mechanics." John Wiley and Sons, Inc., Toronto, Canada.

Rajaratnam, N., Hurtig, K. I. (2000). "Screen-Type Energy Dissipator for Hydraulic Structures." Journal of Hydraulic Engineering, Vol. 126, No. 4, 310-312

Simon, A. L. (1981). "Practical Hydraulics." John Wiley and Sons, Inc., Toronto, Canada.

APPENDIX A

ORIFICEMETER

The discharge measurements were obtained by using an orifice meter designed and assembled according to the Institution of Turkish Standards (TSE) specifications (figure A.1). It is located on the pipe, which transmits the water from the constant head tank to the pressurized tank. The orifice meter includes a mercury manometer inclined with an angle of 30˚.

The principle of the orifice is based on that the reduction of the cross section of the flowing stream in passing through the orifice causes an increase in velocity, which means a decrease in pressure. The manometer inclined with an angle of 30˚ measures the reduction in pressure between the taps.

Energy equation provides a basis for correlating the increase in velocity head with the decrease in pressure head and this correlation provides a way of measuring the flow rate (Munson, Young, and Okiishi (1994)).

If it is assumed that the flow is horizontal, steady, inviscid and incompressible between points (1) and (2), Energy equation becomes

$$\frac{p_1}{\gamma}+\frac{V_1^{\,2}}{2g}=\frac{p_2}{\gamma}+\frac{V_2^{\,2}}{2g}+h_L \qquad \text{(A.1)}$$

The ideal situation has $h_L = 0$. Non-ideal effects occur for two reasons. First, the vena contracta area, A_2, is less than the area of the hole, A_0, by an unknown amount. Thus, $A_2 = C_c A_0$, where C_c is the contraction coefficient (C_c<1). Second, the swirling flow and turbulent motion near the orifice plate introduce a head loss that

cannot be calculated theoretically. As a result, an orifice discharge coefficient, C_0, is used to consider these effects. The equation by which the discharge is calculated is as follows;

$$Q = C_0 Q_{ideal} = C_0 A_0 \sqrt{\frac{2(p_1 - p_2)}{\rho(1-\phi^4)}} \qquad \text{(A.2)}$$

where D_0 is the orifice meter throat diameter, D_1 is the pipe diameter on which the orifice meter located, $\phi = 0.5$ is defined as $\phi = \frac{D_0}{D_1}$ and $A_0 = \frac{\pi D_0^{\,2}}{4}$ is the area of the hole in the orifice plate. The value of C_0 is a function of $\phi = \frac{D_0}{D_1}$ and the Reynolds number $Re = \frac{\rho V_1 D_1}{\mu}$, where $V_1 = \frac{Q}{A_1}$. The value of C_0 depends on the specific construction of the orifice meter.

For the determination of C_0 coefficient, the distinct values given by TSE are used here by fitting a proper trend curve for the discharge calculations (figure A.2).And all the details of the orifice-meter are given in figure A.1.

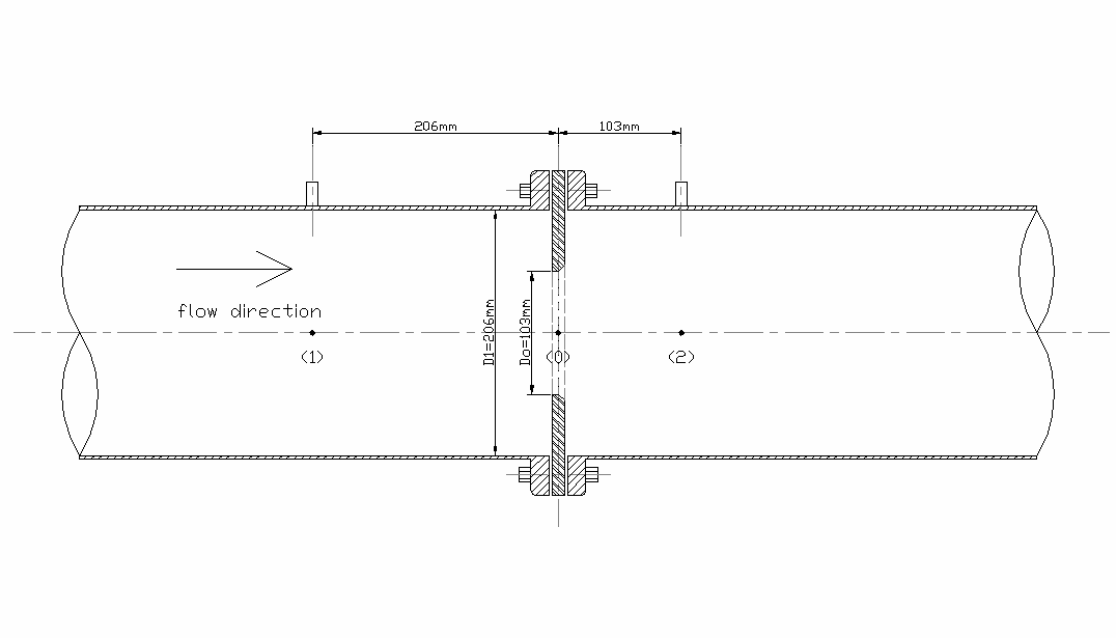

Figure A.1 Details of the orifice-meter

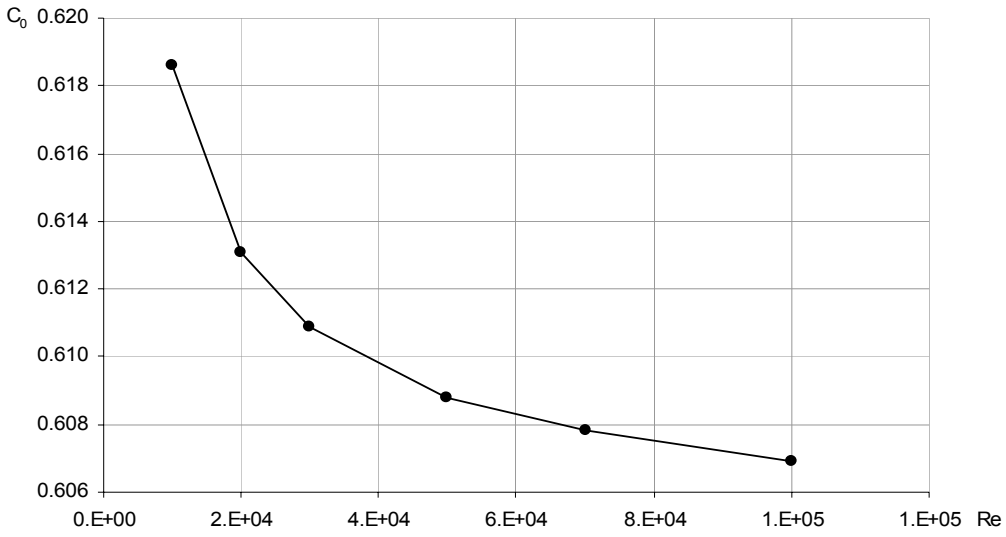

Figure A.2 C_0 vs. *Re* graph for the orifice-meter

APPENDIX B

UNCERTAINTY ANALYSIS OF EXPERIMENTAL DATA

An accepted principle in engineering is that all measurements have errors. By taking this principle into consideration, uncertainty analysis was performed for Q, E_{GC} and S values by using the following basic definitions;

$$\delta R=\left\{\sum_{1}^{n}\left(\left(\partial R/\partial x_i\right)\delta x_i\right)^2\right\}^{\frac{1}{2}} \tag{B.1}$$

$$\delta R=\left\{\sum_{1}^{n}\left[R\left(x_i+\delta x_i\right)-R\left(x_i\right)\right]^2\right\}^{\frac{1}{2}} \tag{B.2}$$

where R represents the result computed from the n measurands $x_1,\ldots,x_i,\ldots,x_n$. δR is the overall uncertainty interval of R and δx_i is the precision error associated with x_i.

B.1 Uncertainty Analysis for Q

In the present study, discharge is calculated by equation A.2 and it can be rewritten as follows;

$$Q = C_0 Q_{ideal} = \frac{C_0 A_0}{(1-\phi^4)^{\frac{1}{2}}}\sqrt{2g\Delta h} \tag{B.3}$$

As can be seen from that equation, Q is computed from one measurand; Δh. Consequently, Equation B.2 can be written for Q values as follows;

$$\delta Q = Q(\Delta h + \delta\Delta h) - Q(\Delta h) \tag{B.4}$$

$$\delta Q = \frac{C_0 A_0}{(1-\phi^4)^{\frac{1}{2}}}\sqrt{2g(\Delta h + \delta\Delta h)} - \frac{C_0 A_0}{(1-\phi^4)^{\frac{1}{2}}}\sqrt{2g(\Delta h)} \tag{B.5}$$

where δΔh is the precision error associated with Δh and equal to $\pm 0.001m$

Overall uncertainty values of δQ_j computed by using Equation B.5 are normalized by the corresponding discharge Q_j and graphically represented by Figure B.1 .(where j is an integer number that represents the number of Q values measured in a given experiment)

As seen in the figure below the relative uncertainty decreases as the Reynolds number increases.

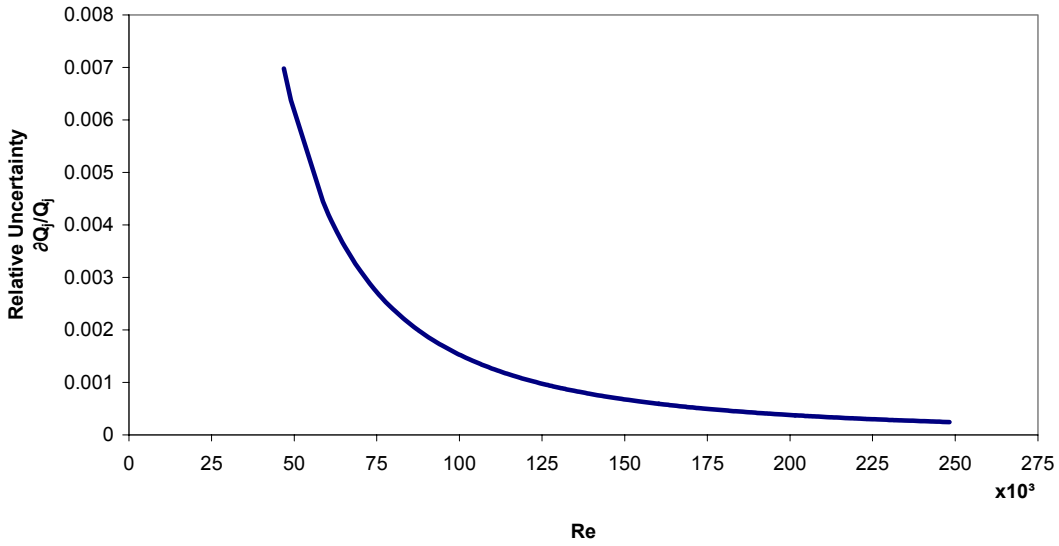

Figure B.1 Relative Uncertainty for Q_j values vs. Re

B.2 Uncertainty Analysis for ΔE_{GC}

In the present study, ΔE_{GC} is calculated by the following equation;

$$\Delta E_{GC}=(y_G+\frac{V_G^2}{2g})-(y_C+\frac{V_C^2}{2g}) \tag{B.6}$$

As can be seen from that equation, ΔE_{GC} is computed from three measurands; Δh, y_C and y_G. Consequently, Equation B.2 can be written for the quantity ΔE_{GC} values as follows;

$$\delta\Delta E_{GC}=\left\{\sum_1^3\left[\Delta E_{GC}\left(x_i+\delta x_i\right)-\Delta E_{GC}\left(x_i\right)\right]^2\right\}^{\frac{1}{2}} \tag{B.7}$$

Equation B.6 can be also written as

$$\delta\Delta E_{GC}=\left\{\left(\Delta E_{GC}(\Delta h+\delta\Delta h)-\Delta E_{GC}(\Delta h,)\right)^2+\left(\Delta E_{GC}(y_C+\delta y_C)-\Delta E_{GC}(y_C)\right)^2+\left(\Delta E_{GC}(y_G+\delta y_G)-\Delta E_{GC}(y_G)\right)^2\right\}^{\frac{1}{2}} \tag{B.8}$$

where $\delta\Delta h$ is the precision error associated with Δh and equal to $\pm 0.001m$, δy_C is the precision error associated with y_C and equal to $\pm 0.0002m$, δy_G is the precision error associated with y_G and equal to $\pm 0.0002m$

Overall uncertainty values of $\delta\Delta E_{GC}$ computed by using Equation B.8 are normalized by the corresponding ΔE_{GC} values and graphically represented by Figure B.2 through Figure B.5

As evident in those Figures overall uncertainty interval for ΔE_{GC} does not exhibit a significant decrease as the Froude number increase in this case.

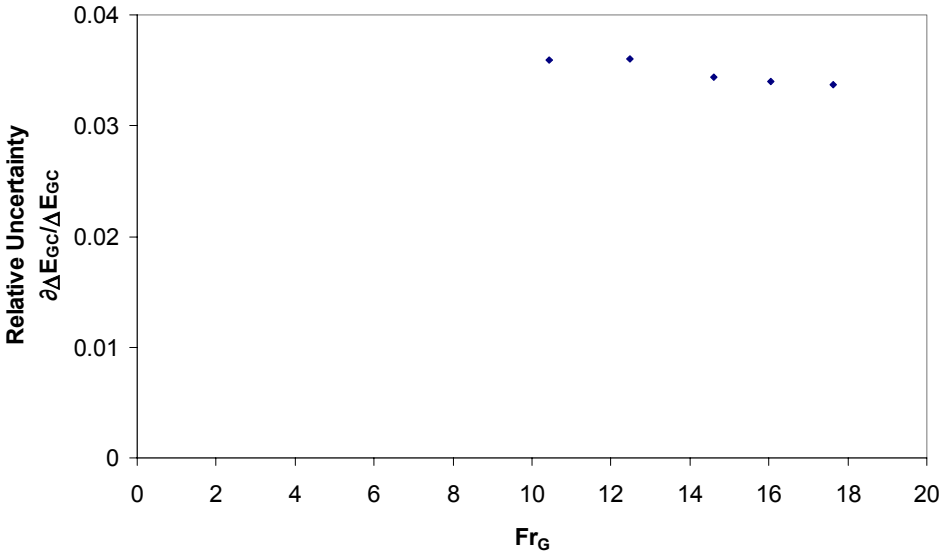

Figure B.2 $\delta\Delta E_{GC}/\Delta E_{GC}$ vs. Fr_G at X/d=50, θ=90º and t/d=2D

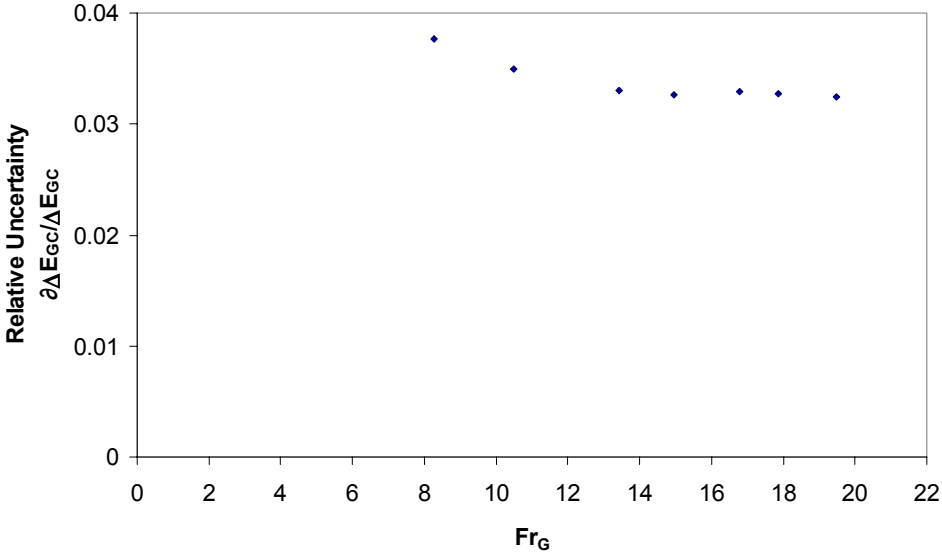

Figure B.3 $\delta\Delta E_{GC}/\Delta E_{GC}$ vs. Fr_G at X/d=50, θ=75º and t/d=2D

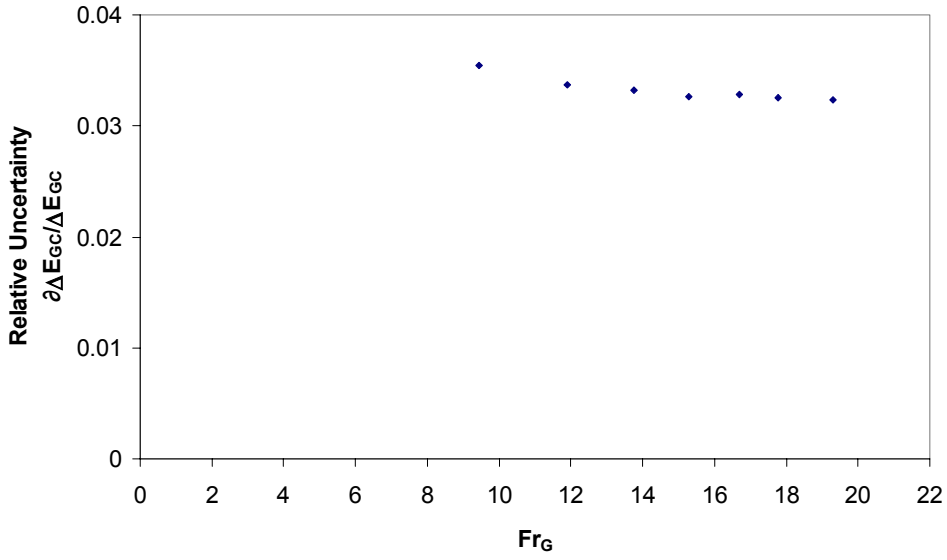

Figure B.4 $\delta\Delta E_{GC}/\Delta E_{GC}$ vs. Fr_G at X/d=50, θ=60º and t/d=2D

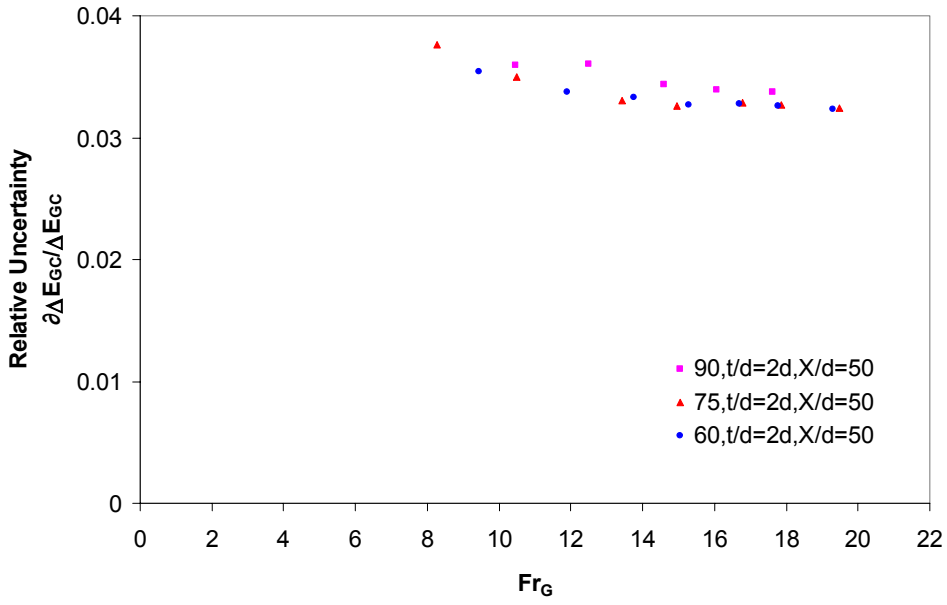

Figure B.5 $\delta\Delta E_{GC}/\Delta E_{GC}$ vs. Fr_G at X/d=50 and t/d=2D for all θ values

B.3 Uncertainty Analysis for S

In the present study, S is calculated by equation B.9 as follows;

$$S = (y_A + \frac{V_A^2}{2g}) - (y_C + \frac{V_C^2}{2g}) - \beta \Delta E_{jA} \qquad \text{(B.9)}$$

β in the above equation is computed from one measurand; x, V_A is computed from two measurands; Δh and y_A, and V_C is computed from two measurands Δh and y_C. This means S is computed from four measurands; x,Δh, y_A and y_C. Then Equation B.2 becomes as follows

$$\delta S = \left\{ \sum_{1}^{4} \left[S(x_i + \delta x_i) - S(x_i) \right]^2 \right\}^{\frac{1}{2}} \qquad \text{(B.10)}$$

where x_1=x and δx_1= δx (the precision error associated with x and equal to $\pm 0.002m$), x_2=Δh and δx_2= $\delta\Delta$h (the precision error associated with Δh and equal to $\pm 0.002m$), x_3=y_A and δx_3=δy_A (the precision error associated with y_A and equal to $\pm 0.0002m$),x_4=y_C and δx_4=δy_C (the precision error associated with y_C and equal to $\pm 0.0002m$).

Overall uncertainty values of δS computed by using Equation B.10 are normalized by the corresponding S values and graphically represented by Figure B.6 through Figure B.9.

Likewise, the overall uncertainty for S does not decrease significantly as Froude number increases.

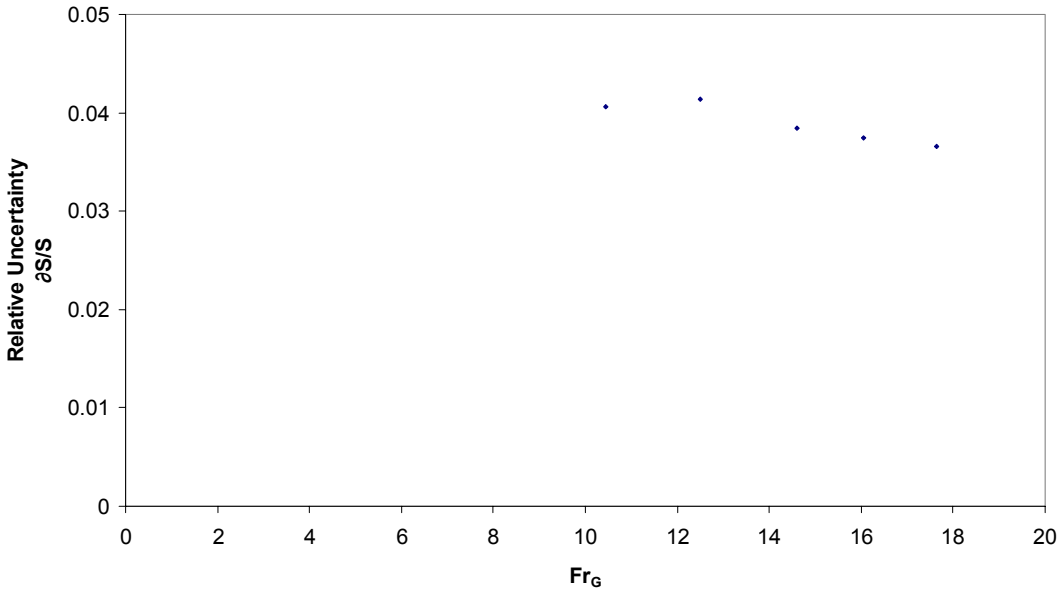

Figure B.6 δS/S vs. Fr_G at X/d=50, θ=90º and t/d=2D

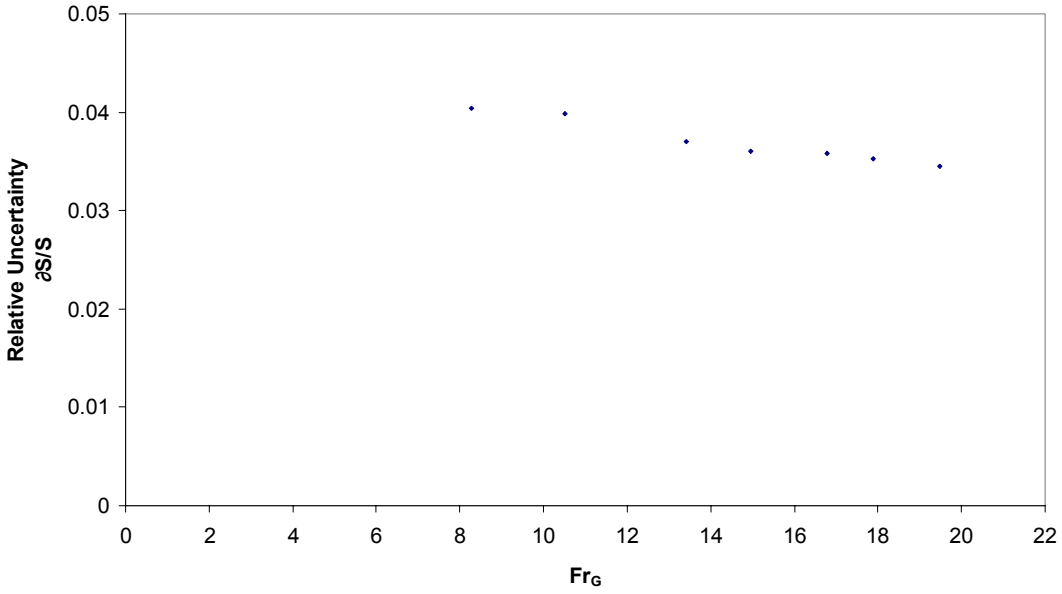

Figure B.7 δS/S vs. Fr_G at X/d=50, θ=75º and t/d=2D

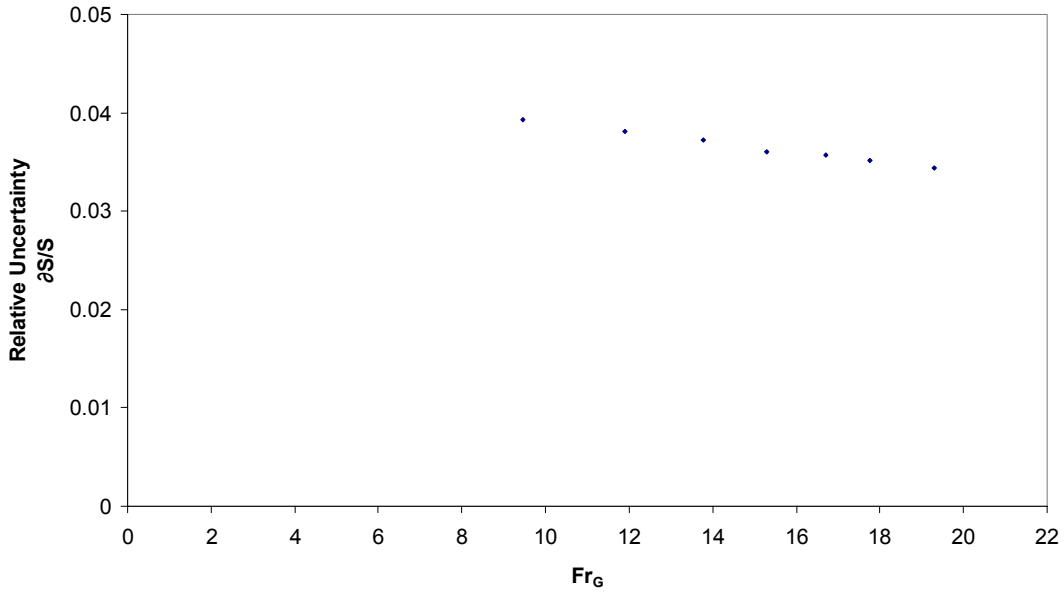

Figure B.8 δS/S vs. Fr_G at X/d=50, θ=60º and t/d=2D

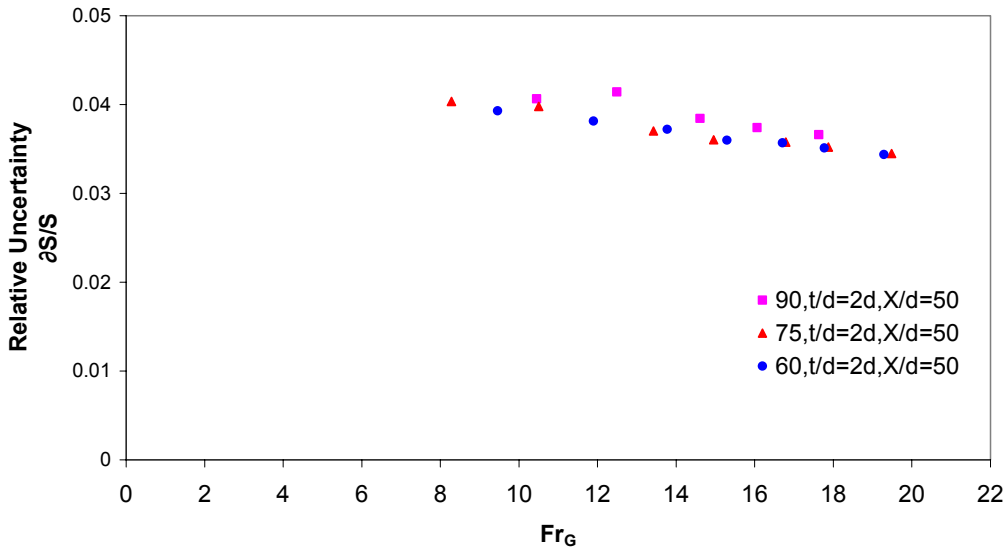

Figure B.9 δS/S vs. Fr_G at X/d=50 and t/d=2D for all θ values

APPENDIX C

EXPERIMENTAL DATA

Table B.1 Experimental Data

Reference	Q(m^3/s)	y_C (cm)	y_A (cm)	S/E_G	$\Delta E_{GC}/E_G$
90-2-100-23.66	0.0300	5.65	2.31	0.164	0.948
90-2-100-10.23	0.0116	3.62	1.53	0.058	0.872
90-2-100-21.39	0.0271	5.35	2.06	0.208	0.941
90-2-100-12.89	0.0164	4.10	1.65	0.237	0.894
90-2-100-16.82	0.0247	5.14	1.79	0.346	0.921
90-2-100-15.55	0.0201	4.85	1.79	0.246	0.920
90-2-100-16.44	0.0222	5.06	1.91	0.241	0.924
90-2-50-24.02	0.0270	4.60	1.15	0.738	0.939
90-2-50-12	0.0132	8.06	1.14	0.607	0.906
90-2-50-21.57	0.0252	4.66	1.18	0.731	0.935
90-2-50-15.42	0.0181	4.54	1.19	0.685	0.920
90-2-50-18.94	0.0229	4.73	1.21	0.720	0.930
90-2-50-17.08	0.0198	4.84	1.18	0.708	0.930
90-2-50-17.1	0.0214	4.67	1.24	0.706	0.923
60-2-100-17.24	0.0319	5.87	2.59	0.191	0.920
60-2-100-6.59	0.0085	3.56	1.72	0.079	0.802
60-2-100-15.38	0.0284	5.92	2.10	0.344	0.916
60-2-100-11.77	0.0135	3.82	1.63	0.058	0.888
60-2-100-15.39	0.0244	5.63	1.86	0.349	0.921
60-2-100-15.33	0.0206	4.32	1.92	0.205	0.905
60-2-100-14.34	0.0179	5.08	1.74	0.234	0.921
60-2-50-22.45	0.0296	4.81	1.28	0.725	0.931
60-2-50-11.33	0.0124	8.00	1.13	0.520	0.897
60-2-50-20.5	0.0270	4.73	1.28	0.715	0.927
60-2-50-15.5	0.0168	4.43	1.13	0.645	0.922
60-2-50-21.85	0.0250	4.34	1.17	0.715	0.930
60-2-50-18.84	0.0207	3.22	1.14	0.652	0.888
60-2-50-19.42	0.0229	4.84	1.19	0.709	0.934
90-1-100-16.57	0.0244	4.04	1.63	0.345	0.890
90-1-100-10.77	0.0118	2.97	1.52	0.077	0.848
90-1-100-14.2	0.0214	3.62	1.76	0.253	0.860
90-1-100-12.08	0.0150	2.98	1.66	0.108	0.837
90-1-100-14.84	0.0201	3.88	1.74	0.223	0.888

Table B.1 Experimental Data (continued)

Reference	Q(m^3/s)	y_C (cm)	y_A (cm)	S/E_G	$\Delta E_{GC}/E_G$
90-1-100-13.42	0.0170	3.71	1.77	0.149	0.883
90-1-100-14.82	0.0187	3.76	1.54	0.274	0.891
60-1-100-17.69	0.0267	4.99	1.64	0.403	0.919
60-1-100-8.77	0.0110	5.43	1.24	0.119	0.869
60-1-100-15.99	0.0244	5.40	1.63	0.434	0.921
60-1-100-12.37	0.0156	4.48	1.67	0.184	0.901
60-1-100-16.44	0.0222	4.84	1.71	0.293	0.920
60-1-100-13.26	0.0185	4.56	1.79	0.210	0.901
60-1-100-15.81	0.0202	4.78	1.75	0.231	0.920
90-1-50-16.86	0.0230	3.85	1.31	0.660	0.890
90-1-50-6.43	0.0089	4.50	1.31	0.285	0.806
90-1-50-16.56	0.0214	4.10	1.27	0.666	0.905
90-1-50-8.59	0.0123	3.60	1.31	0.614	0.832
90-1-50-14.49	0.0198	4.11	1.31	0.637	0.895
90-1-50-13.58	0.0160	3.82	1.19	0.597	0.895
90-1-50-12.4	0.0182	4.15	1.38	0.599	0.881
75-1-50-16.8	0.0230	3.57	1.31	0.645	0.876
75-1-50-8.03	0.0106	7.01	1.29	0.381	0.841
75-1-50-15.75	0.0215	3.75	1.31	0.642	0.884
75-1-50-7.86	0.0135	7.99	1.53	0.444	0.839
75-1-50-14.49	0.0198	3.51	1.31	0.611	0.868
75-1-50-13.36	0.0179	3.72	1.30	0.598	0.877
75-1-50-12.73	0.0162	3.65	1.25	0.576	0.878
60-1-50-20.68	0.0233	3.92	1.15	0.697	0.918
60-1-50-10.49	0.0118	7.21	1.16	0.491	0.890
60-1-50-16.52	0.0210	3.91	1.25	0.659	0.900
60-1-50-11.15	0.0135	8.19	1.21	0.540	0.896
60-1-50-15.18	0.0198	4.06	1.27	0.645	0.899
60-1-50-13.38	0.0159	4.17	1.20	0.603	0.903
60-1-50-13.57	0.0179	4.07	1.28	0.616	0.893
75-1-100-16.1	0.0232	4.48	1.61	0.347	0.906
75-1-100-9.71	0.0111	3.56	1.66	0.052	0.864
75-1-100-14.13	0.0215	4.86	1.75	0.276	0.905
75-1-100-11.89	0.0138	3.41	1.68	0.068	0.872
75-1-100-14.12	0.0199	4.81	1.75	0.223	0.909
75-1-100-12.39	0.0158	4.44	1.65	0.233	0.900
75-1-100-13.22	0.0180	4.50	1.73	0.256	0.901
90-2D-100-19.25	0.0258	6.63	1.56	0.376	0.947
90-2D-100-9.48	0.0124	3.60	1.28	0.083	0.851
90-2D-100-11.55	0.0151	4.44	1.36	0.095	0.893
90-2D-100-15.66	0.0230	5.64	1.59	0.347	0.926
90-2D-100-13.12	0.0180	4.76	1.59	0.212	0.906
90-2D-100-14.2	0.0214	6.14	1.64	0.345	0.924
90-2D-100-13.12	0.0198	5.36	1.57	0.352	0.910
75-2D-100-19.27	0.0259	7.37	1.67	0.318	0.951
75-2D-100-10.19	0.0137	4.85	1.30	0.103	0.886

Table B.1 Experimental Data (continued)

Reference	Q(m³/s)	y_C (cm)	y_A (cm)	S/E_G	$\Delta E_{GC}/E_G$
75-2D-100-13.15	0.0164	5.30	1.61	0.065	0.917
75-2D-100-14.35	0.0226	6.33	1.65	0.343	0.925
75-2D-100-14.6	0.0193	5.39	1.58	0.242	0.923
60-2D-100-16.91	0.0258	6.05	1.73	0.329	0.932
60-2D-100-7.48	0.0114	5.48	1.41	0.129	0.840
60-2D-100-14.44	0.0238	6.85	1.58	0.436	0.927
60-2D-100-9.39	0.0143	5.96	1.41	0.114	0.880
60-2D-100-15.87	0.0214	6.81	1.50	0.349	0.938
60-2D-100-13.01	0.0170	5.84	1.31	0.151	0.919
60-2D-100-13.17	0.0193	5.15	1.57	0.279	0.909
90-2D-50-17.64	0.0223	5.85	1.25	0.708	0.940
90-2D-50-10.45	0.0132	6.80	1.25	0.524	0.894
90-2D-50-16.07	0.0203	5.78	1.25	0.687	0.934
90-2D-50-12.5	0.0158	4.03	1.25	0.582	0.891
90-2D-50-14.61	0.0185	5.35	1.25	0.658	0.925
75-2-100-15.9	0.0246	5.17	1.82	0.325	0.916
75-2-100-7.28	0.0113	7.28	1.43	0.117	0.820
75-2-100-16.59	0.0231	5.27	1.72	0.315	0.926
75-2-100-12.4	0.0146	7.26	1.67	0.157	0.915
75-2-100-13.43	0.0214	5.33	1.93	0.255	0.908
75-2-100-12.98	0.0171	8.78	1.82	0.183	0.918
75-2-100-12.78	0.0194	5.27	1.91	0.216	0.907
75-2-50-15.96	0.0238	4.21	1.39	0.663	0.894
75-2-50-7.84	0.0117	7.73	1.39	0.400	0.833
75-2-50-16.27	0.0224	4.21	1.32	0.667	0.902
75-2-50-11.75	0.0145	7.64	1.23	0.574	0.908
75-2-50-15.57	0.0206	4.15	1.29	0.655	0.902
75-2-50-13.13	0.0167	4.03	1.25	0.600	0.893
75-2-50-14.49	0.0188	3.88	1.27	0.627	0.891
75-2D-50-19.49	0.0261	5.66	1.30	0.724	0.940
75-2D-50-8.29	0.0111	7.66	1.30	0.399	0.842
75-2D-50-17.88	0.0240	5.45	1.30	0.709	0.934
75-2D-50-10.51	0.0141	8.80	1.30	0.532	0.885
75-2D-50-16.8	0.0225	5.32	1.30	0.696	0.929
75-2D-50-13.43	0.0180	8.12	1.30	0.647	0.924
75-2D-50-14.96	0.0201	8.74	1.30	0.681	0.934
60-2D-50-19.29	0.0259	5.99	1.30	0.726	0.943
60-2D-50-9.46	0.0127	6.96	1.30	0.486	0.878
60-2D-50-17.78	0.0238	5.69	1.30	0.711	0.936
60-2D-50-11.9	0.0160	7.97	1.30	0.598	0.910
60-2D-50-16.71	0.0224	5.50	1.30	0.697	0.931
60-2D-50-13.78	0.0185	10.36	1.30	0.649	0.920
60-2D-50-15.3	0.0205	10.19	1.30	0.685	0.933
75-1-50-10.05	0.0349	7.95	3.02	0.312	0.874
75-1-50-13.79	0.0446	9.56	3.25	0.294	0.918

Table B.1 Experimental Data (continued)

Reference	Q(m^3/s)	y_C (cm)	y_A (cm)	S/E_G	$\Delta E_{GC}/E_G$
75-1-50-5.39	0.0194	5.78	2.50	0.126	0.736
75-1-50-12.11	0.0393	9.21	3.11	0.302	0.906
75-1-50-6.45	0.0232	5.93	2.50	0.106	0.774
75-1-50-10.83	0.0366	8.05	2.76	0.409	0.884
75-1-50-6.99	0.0251	6.33	2.50	0.119	0.798
75-1-50-9.73	0.0329	8.14	2.87	0.334	0.874
75-1-50-8.78	0.0274	6.57	2.48	0.245	0.846
75-1-50-8.76	0.0311	7.34	2.86	0.297	0.849
75-1-50-9.07	0.0288	6.28	2.44	0.359	0.842
75-1-50-9.41	0.0302	7.19	3.04	0.202	0.863
90-1-50-10.4	0.0419	8.96	2.86	0.522	0.879
90-1-50-11.25	0.0398	8.75	3.29	0.289	0.892
90-1-50-5.48	0.0197	5.31	2.50	0.106	0.723
90-1-50-11.17	0.0377	8.70	3.10	0.306	0.893
90-1-50-6.24	0.0224	5.89	2.50	0.109	0.767
90-1-50-10.01	0.0348	7.97	2.73	0.415	0.874
90-1-50-7.7	0.0251	6.24	3.25	0.103	0.819
90-1-50-9.74	0.0328	7.62	3.04	0.271	0.869
90-1-50-9.66	0.0271	6.41	2.81	0.204	0.862
90-1-50-10.86	0.0308	7.25	3.15	0.177	0.886
90-1-50-7.67	0.0291	6.85	2.88	0.314	0.817
60-1-50-10.64	0.0440	10.05	3.25	0.424	0.890
60-1-50-5.51	0.0198	5.25	2.50	0.103	0.721
60-1-50-9.75	0.0409	9.83	3.34	0.384	0.878
60-1-50-6.45	0.0232	6.22	2.50	0.114	0.782
60-1-50-9.89	0.0390	9.16	3.26	0.361	0.878
60-1-50-7.14	0.0257	6.40	2.50	0.131	0.803
60-1-50-9.81	0.0368	8.91	3.27	0.321	0.877
60-1-50-9.04	0.0291	7.00	3.10	0.177	0.855
60-1-50-9.3	0.0345	8.55	3.00	0.377	0.868
60-1-50-8.32	0.0305	7.25	3.19	0.236	0.839
60-1-50-9.34	0.0333	7.91	3.45	0.214	0.864
90-1-100-10.25	0.0441	9.58	3.55	0.331	0.880
90-1-100-7.31	0.0237	6.28	2.34	0.109	0.813
90-1-100-10.26	0.0423	9.75	3.55	0.306	0.884
90-1-100-8.24	0.0270	6.98	3.11	0.071	0.842
90-1-100-9.21	0.0404	9.13	3.60	0.322	0.863
90-1-100-8.56	0.0288	7.41	3.30	0.076	0.851
90-1-100-9.59	0.0383	8.77	3.64	0.242	0.870
90-1-100-9.18	0.0312	7.28	3.23	0.187	0.857
90-1-100-9.33	0.0364	8.38	3.48	0.263	0.864
90-1-100-8.54	0.0333	7.86	3.42	0.222	0.847
90-1-100-8.93	0.0346	8.20	3.50	0.243	0.857
75-1-100-12.37	0.0436	9.13	3.37	0.273	0.903
75-1-100-6.65	0.0239	6.24	2.50	0.110	0.788

Table B.1 Experimental Data (continued)

Reference	Q(m³/s)	y_C (cm)	y_A (cm)	S/E_G	$\Delta E_{GC}/E_G$
75-1-100-10.17	0.0397	9.03	3.50	0.266	0.880
75-1-100-9.09	0.0307	7.45	3.31	0.063	0.859
75-1-100-9.62	0.0365	8.48	3.44	0.232	0.870
75-1-100-8.52	0.0337	7.91	3.31	0.166	0.846
60-1-100-9.86	0.0435	10.51	3.45	0.377	0.881
60-1-100-7.81	0.0276	6.84	2.48	0.105	0.826
60-1-100-9.75	0.0408	8.78	3.50	0.307	0.869
60-1-100-9.8	0.0314	7.45	3.08	0.064	0.870
60-1-100-9.96	0.0388	8.63	3.49	0.245	0.874
60-1-100-8.6	0.0338	7.76	3.20	0.116	0.846
60-1-100-9.19	0.0368	7.98	3.44	0.230	0.855
60-1-100-9.15	0.0351	7.83	3.32	0.170	0.856
90-0.5-50-10.64	0.0435	8.97	2.80	0.517	0.881
90-0.5-50-6.84	0.0225	5.82	2.89	0.156	0.790
90-0.5-50-9.95	0.0405	8.98	2.70	0.568	0.875
90-0.5-50-7.12	0.0271	6.33	2.96	0.307	0.793
90-0.5-50-8.82	0.0376	8.10	3.02	0.437	0.847
90-0.5-50-8.8	0.0307	7.76	3.19	0.268	0.857
90-0.5-50-8.53	0.0353	8.69	3.28	0.333	0.853
90-0.5-50-8.93	0.0331	7.53	3.25	0.264	0.851
60-0.5-50-9.86	0.0398	7.41	2.99	0.423	0.850
60-0.5-50-6.84	0.0246	6.18	3.01	0.099	0.790
60-0.5-50-8.61	0.0373	7.61	3.00	0.458	0.834
60-0.5-50-7.86	0.0278	6.86	2.95	0.298	0.828
60-0.5-50-9.39	0.0341	7.90	3.29	0.273	0.864
60-0.5-50-8.72	0.0319	7.60	3.25	0.276	0.851
60-0.5-50-8.91	0.0306	6.95	3.25	0.234	0.847
60-0.5-50-8.8	0.0293	7.67	3.19	0.253	0.859
75-0.5-50-9.31	0.0396	8.05	2.87	0.507	0.852
75-0.5-50-7.23	0.0237	6.24	2.97	0.097	0.810
75-0.5-50-9.72	0.0372	7.79	3.12	0.339	0.861
75-0.5-50-7.64	0.0271	6.22	3.00	0.263	0.808
75-0.5-50-9.17	0.0344	7.76	3.09	0.357	0.857
75-0.5-50-8.61	0.0297	6.77	2.95	0.308	0.839
75-0.5-50-9.61	0.0329	7.06	3.22	0.247	0.857
75-0.5-50-8.77	0.0314	7.02	3.27	0.250	0.843
90-0.5-100-11.71	0.0425	9.65	3.55	0.233	0.901
90-0.5-100-7.49	0.0236	6.63	2.85	0.084	0.826
90-0.5-100-11.16	0.0401	8.63	3.60	0.207	0.889
90-0.5-100-8.12	0.0274	7.19	3.46	0.062	0.841
90-0.5-100-9.74	0.0376	8.53	3.54	0.244	0.871
90-0.5-100-9.42	0.0309	7.25	3.27	0.167	0.862
90-0.5-100-9.71	0.0351	8.08	3.54	0.204	0.870
90-0.5-100-9.44	0.0333	7.79	3.35	0.219	0.865
75-0.5-100-9.22	0.0422	9.98	3.55	0.318	0.868

Table B.1 Experimental Data (continued)

Reference	Q(m^3/s)	y_C (cm)	y_A (cm)	S/E_G	$\Delta E_{GC}/E_G$
75-0.5-100-8.51	0.0279	6.95	3.16	0.065	0.845
75-0.5-100-10.42	0.0372	8.98	3.53	0.223	0.886
75-0.5-100-9.59	0.0310	7.48	3.41	0.093	0.868
75-0.5-100-9.8	0.0350	8.53	3.47	0.230	0.876
75-0.5-100-10.2	0.0331	8.18	3.42	0.177	0.882
60-0.5-100-11.65	0.0420	10.53	3.51	0.267	0.906
60-0.5-100-8.14	0.0261	6.75	2.99	0.072	0.839
60-0.5-100-10.33	0.0400	9.06	3.60	0.254	0.882
60-0.5-100-9.01	0.0296	7.45	3.30	0.063	0.860
60-0.5-100-10.2	0.0378	9.32	3.61	0.225	0.885
60-0.5-100-9.49	0.0328	7.91	3.51	0.132	0.868
60-0.5-100-10.97	0.0354	8.45	3.56	0.195	0.892
60-0.5-100-9.78	0.0341	8.15	3.38	0.220	0.873
90-1D-100-11.15	0.0425	9.72	3.73	0.089	0.895
90-1D-100-8.8	0.0339	8.08	2.62	0.103	0.854
90-1D-100-11.76	0.0417	9.40	3.41	0.123	0.901
90-1D-100-9.74	0.0358	8.40	2.87	0.085	0.873
90-1D-100-11.22	0.0404	9.18	3.24	0.067	0.895
90-1D-100-10.14	0.0375	8.58	2.82	0.085	0.878
90-1D-100-10.82	0.0393	9.13	3.26	0.069	0.891
90-1D-100-10.55	0.0385	8.57	3.32	0.064	0.883
75-1D-100-11.09	0.0450	9.98	3.64	0.140	0.894
75-1D-100-10.35	0.0371	8.43	2.50	0.094	0.881
75-1D-100-12.14	0.0438	9.51	3.27	0.128	0.904
75-1D-100-12.18	0.0387	8.63	2.31	0.085	0.903
75-1D-100-11.66	0.0419	9.17	3.19	0.065	0.898
75-1D-100-11.95	0.0400	8.60	2.42	0.083	0.899
75-1D-100-11.48	0.0409	8.92	2.60	0.084	0.895
60-1D-100-11.83	0.0434	9.26	3.49	0.058	0.899
60-1D-100-10.69	0.0384	8.58	2.50	0.092	0.885
60-1D-100-11.88	0.0415	8.87	2.46	0.085	0.898
60-1D-100-12.12	0.0396	8.85	2.35	0.086	0.903
60-1D-100-12.43	0.0403	8.88	2.34	0.084	0.906
90-1D-50-12.5	0.0444	10.33	2.48	0.529	0.912
90-1D-50-9.33	0.0332	7.72	2.48	0.294	0.862
90-1D-50-12.42	0.0430	9.76	2.44	0.465	0.909
90-1D-50-9.35	0.0350	8.41	2.57	0.375	0.867
90-1D-50-11.4	0.0408	9.39	2.49	0.479	0.898
90-1D-50-11.17	0.0374	8.88	2.38	0.465	0.895
90-1D-50-11.8	0.0393	8.99	2.38	0.476	0.901
75-1D-50-11.89	0.0428	10.79	2.50	0.526	0.909
75-1D-50-9.51	0.0341	8.07	2.50	0.282	0.868
75-1D-50-10.74	0.0371	9.22	2.44	0.379	0.893
75-1D-50-11.35	0.0410	10.22	2.51	0.484	0.902
75-1D-50-10.79	0.0387	9.41	2.49	0.468	0.893

Table B.1 Experimental Data (continued)

Reference	Q(m³/s)	y_C (cm)	y_A (cm)	S/E_G	$\Delta E_{GC}/E_G$
60-1D-50-10.76	0.0349	8.26	2.34	0.354	0.888
60-1D-50-11.26	0.0420	10.08	2.60	0.505	0.899
60-1D-50-11.53	0.0370	8.59	2.41	0.417	0.898
60-1D-50-12.2	0.0404	9.70	2.49	0.449	0.909
60-1D-50-12	0.0387	9.95	2.49	0.432	0.909